Version of Record: https://www.sciencedirect.com/science/article/pii/S1568988321001104
Manuscript_ab014d4cb1953428970c0e4fa0d3f49f

The Lake Erie HABs Grab: A binational collaboration to characterize the western basin cyanobacterial harmful algal blooms at an unprecedented high-resolution spatial scale

Justin D. Chaffin[a,*], John F. Bratton[b], Edward M. Verhamme[b], Halli B. Bair[a,1], Amber A. Beecher[c], Caren E. Binding[d], Johnna A. Birbeck[e], Thomas B. Bridgeman[c], Xuexiu Chang[f,g], Jill Crossman[h], Warren J.S. Currie[i], Timothy W. Davis[j], Gregory J. Dick[k], Kenneth G. Drouillard[f], Reagan M. Errera[l], Thijs Frenken[f, 2], Hugh J. MacIsaac[f], Andrew McClure[m], R. Michael McKay[f], Laura A. Reitz[j,3], Jorge W. Santo Domingo[n], Keara Stanislawczyk[a], Richard P. Stumpf[o], Zachary D. Swan[c], Brenda K. Snyder[c], Judy A. Westrick[e], Pengfei Xue[p], Colleen E. Yancey[k], Arthur Zastepa[d], Xing Zhou[p]

a: F.T. Stone Laboratory and Ohio Sea Grant, The Ohio State University, 878 Bayview Ave. P.O. Box 119, Put-In-Bay, OH 43456, USA

b: LimnoTech, 501 Avis Drive, Ann Arbor, MI 48108, USA

c: Lake Erie Center, University of Toledo, 6200 Bayshore Rd., Oregon, OH 43616, USA

d: Environment and Climate Change Canada, Canada Centre for Inland Waters, 867 Lakeshore Road, Burlington, Ontario, L7S1A1, Canada

e: Lumigen Instrument Center, Wayne State University, 5101Cass Ave., Detroit, MI 48202, USA

f: Great Lakes Institute for Environmental Research, University of Windsor, 401 Sunset Ave. Windsor, Ontario, N9B 3P4, Canada

g: School of Ecology and Environmental Sciences, Yunnan University, Kunming 650091, P. R. China

h: School of the Environment, University of Windsor, 401 Sunset Avenue, Windsor, Ontario, N9B 3P4, Canada

i: Fisheries and Oceans Canada, Canada Centre for Inland Waters, 867 Lakeshore Rd., Burlington, Ontario, L7S 1A1, Canada

j: Biological Sciences, Bowling Green State University, Life Sciences Building, Bowling Green, OH 43402, United States

k: Department of Earth and Environmental Sciences, University of Michigan, 2534 North University Building, 1100 North University Avenue, Ann Arbor, MI 48109-1005, USA

l: Great Lakes Environmental Research Laboratory, National Oceanic and Atmospheric Administration, Ann Arbor, MI 48108, USA

m: Division of Water Treatment, City of Toledo, Toledo, OH 43605, USA

n: United States Environmental Protection Agency, Cincinnati, OH, 45268, USA

o: National Ocean Service, National Oceanic and Atmospheric Administration, 1305 East West Highway, Silver Spring, MD 20910, USA

p: Civil and Environmental Engineering, Michigan Technological University, 1400 Townsend Dr., Houghton, MI 49931, USA

*corresponding author: chaffin.46@osu.edu, 419-285-1845

1 Current Address: Department of Civil Engineering, Ohio University, Athens, OH 45701, USA

2 Current Address: Department of Aquatic Ecology, Netherlands Institute of Ecology (NIOO-KNAW), Droevendaalsesteeg 10, 6708 PB, Wageningen, The Netherlands

3 Current Address: Department of Earth and Environmental Sciences, University of Michigan, 2534 North University Building, 1100 North University Avenue, Ann Arbor, MI 48109-1005, USA

Keywords

Cyanobacteria, eutrophication, environmental monitoring, international collaboration, *Microcystis*, microcystin

Abstract

Monitoring of cyanobacterial bloom biomass in large lakes at high resolution is made possible by remote sensing. However, monitoring cyanobacterial toxins is only feasible with grab samples, which, with only sporadic sampling, results in uncertainties in the spatial distribution of toxins. To address this issue, we conducted two intensive "HABs Grabs" of microcystin (MC)-producing *Microcystis* blooms in the western basin of Lake Erie. These were one-day sampling events during August of 2018 and 2019 in which 100 and 172 grab samples were collected, respectively, within a six-hour window covering up to 2,270 km^2 and analyzed using consistent methods to estimate the total mass of MC. The samples were analyzed for 57 parameters, including toxins, nutrients, chlorophyll, and genomics. There were an estimated 11,513 kg and 30,691 kg of MCs in the western basin during the 2018 and 2019 HABs Grabs, respectively. The bloom boundary poses substantial issues for spatial assessments because MC concentration varied by nearly two orders of magnitude over very short distances. The MC to chlorophyll ratio (MC:chl) varied by a factor up to 5.3 throughout the basin, which creates challenges for using MC:chl to predict MC concentrations. Many of the biomass metrics strongly correlated ($r > 0.70$) with each other except chlorophyll fluorescence and phycocyanin concentration. While MC and chlorophyll correlated well with total phosphorus and nitrogen concentrations, MC:chl correlated with dissolved inorganic nitrogen. More frequent MC data collection can overcome these issues, and models need to account for the MC:chl spatial heterogeneity when forecasting MCs.

1. Introduction

Harmful algal blooms (HABs) are a global issue and are a growing concern due to their documented expansion driven by increased anthropogenic nutrient pollution and climate change (O'Neil et al., 2012; Paerl et al., 2016). Many human health, ecological, and economic problems are associated with HABs, but a significant risk is the toxin contamination of recreational and drinking waters by freshwater cyanobacterial HABs (cyanoHABs) (Carmichael, 1992; He et al., 2016; Qin et al., 2010; Sitoki et al., 2012; Steffen et al., 2017). Among the many types of toxins produced by cyanoHABs, microcystins (MCs) are the most commonly documented and often found in the highest concentrations (Carmichael and Boyer, 2016; Graham et al., 2020; Harke et al., 2016; Loftin et al., 2016). During bloom conditions, MC concentrations can exceed the World Health Organization (WHO) and local government guidelines for drinking water and recreational uses by several orders of magnitude (Davis et al., 2019; Krausfeldt et al., 2019). Several major cities worldwide have recently issued 'do not drink advisories' due to MCs in treated tap water (Qin et al., 2010; Sitoki et al., 2012; Steffen et al., 2017). Annual summertime cyanoHABs dominated by *Microcystis*, a globally distributed MC-producer (Harke et al., 2016), have plagued Lake Erie's western basin for the past two decades (Bridgeman et al., 2013; Steffen et al., 2014; Stumpf et al., 2012). In August 2014, the City of Toledo issued a three-day do not drink advisory due to MCs in tap water, which affected nearly 500,000 residents (Qian et al., 2015; Steffen et al., 2017). Although the 2014 Lake Erie cyanoHAB was not particularly expansive compared to previous years (Davis et al., 2019), the accumulation of MC-producing cyanoHAB biomass at Toledo's drinking water intake posed a threat to human health. Therefore, the development of forecasting capabilities for cyanoHAB toxins is paramount to protect human health and mitigate the multiple negative impacts of blooms.

Unlike monitoring for MCs, monitoring the biomass of annual cyanoHABs is made possible over large areas and over time by remote sensing. Airborne or satellite remote sensing allows for surface cyanoHAB biomass in lakes to be quantified with high spatial resolution and frequent revisits (Wynne and Stumpf, 2015). Regular (daily to weekly) satellite images of a lake allow for an annual assessment of cyanoHAB biomass, and multiple years of images document interannual trends and variability. Throughout the Lake Erie bloom season, the U.S. National Oceanic and Atmospheric Administration (NOAA) disseminates semi-weekly bulletins that display bloom location and biomass quantified by remote sensing. The bulletins also forecast the bloom's location over the next several days using wind predictions and resulting water currents (Wynne et al., 2013). Additionally, Environment and Climate Change Canada's (ECCC) EOLakeWatch delivers a suite of satellite-derived products for Lake Erie, mapping total chlorophyll *a* and providing quantitative indices describing the bloom spatial extent, intensity, and duration (Binding et al., 2021). Coupling the extensive satellite-derived biomass data with an examination of environmental drivers has led to the development of regression models and mechanistic models driven by springtime Maumee River cumulative discharge and phosphorus loading (GLWQA, 2015; Sayers et al., 2016; Stumpf et al., 2016b; Verhamme et al., 2016). These models largely explain the interannual variability of cyanoHAB biomass and allow for seasonal predictions months in advance of the actual bloom (Stumpf et al., 2012).

Unfortunately, neither ECCC nor NOAA remote sensing products and bulletins include annual MC assessments or MC forecasts because cyanoHAB toxins cannot be directly detected through remote sensing (Stumpf et al., 2016a). Neither may cyanoHAB biomass be used as a proxy for MC concentration because blooms comprise both MC-producing and non-MC-producing strains, and there is no consistent correlation between cyanoHAB biomass and MC

concentration (Liu et al., 2020; Stumpf et al., 2016a). Therefore, in order to estimate the mass of MCs throughout a lake or basin and develop annual assessments of toxicity and predictive models, in the same manner that remote sensing has allowed for cyanoHAB biomass, extensive MC data acquired by vessel-based water grab samples are needed.

Collecting water samples at sufficiently high spatial resolution in Lake Erie so that MC data might be reasonably compared with satellite cyanoHAB biomass data is a formidable challenge. Lake Erie is the 11th largest lake in the world by surface area (Herdendorf, 1982), and the western basin, where cyanoHABs are most prevalent, has an area of approximately 3,000 km^2. Two U.S. states (Ohio and Michigan) and a Canadian province (Ontario) have jurisdiction over the western basin's waters, thus making the cyanoHABs an international problem. While the management of environmental problems that span international boundaries can be challenging (Perz et al., 2010), the U.S. and Canada have a long history of collaboration on the Great Lakes (e.g., International Joint Commission, Great Lakes Water Quality Agreement, Great Lakes Fisheries Commission; McKindles et al., 2020). While many researchers and agencies are studying Lake Erie's cyanoHABs, the basin's large size and multiple jurisdictions lead to discrepancies in grab sample collection and analysis methods for routine monitoring, making data amalgamation difficult (Golnick et al., 2016). Some researchers (Fang et al., 2019) have pooled cyanoHAB biomass data from the various institutions to make annual assessments, but correction factors need to be introduced and caveats acknowledged to make the combined dataset useful. Thousands of grab samples from Lake Erie have been analyzed for MCs in recent years, but before those data can be combined to make spatial assessments of MCs throughout the lake, a tool is needed to quantify the uncertainty associated with pooling multiple sources of MCs data. As part of a more extensive multi-institution study oriented toward developing forecasting

of conditions favorable for MC production by Lake Erie cyanoHABs, investigators determined that the study would benefit from the collection of one or more MCs datasets from a high spatial resolution survey with coordinated methods collected across the lake basin. Such a dataset was expected to allow for calculating the total mass and the average concentration of MCs in the basin at a single point in time, which would be analogous to a satellite image displaying cyanoHAB biomass.

This study's primary objective was to coordinate two six-hour, high-resolution sampling events on Lake Erie's western basin to estimate the total mass of MCs during the peaks of the annual cyanoHAB on 9 August 2018 and 7 August 2019. We termed these one-day sampling events "HABs Grabs." The 2018 HABs Grab had a smaller number of participating institutions and was limited to the U.S. waters. Due to the attention of the initial HABs Grab, Canadian institutions also participated in 2019. Additionally, because HABs Grab partners have a wide range of expertise on cyanoHABs (molecular scale to ecosystem modeling), the HABs Grab represented an opportunity to collect data to answer many additional scientific questions. All HABs Grab samples were collected and analyzed for 57 different parameters by consistent methods, including toxins, pigments, nutrients, and cyanobacterial DNA. In this manuscript, we present: 1) the coordination elements of the HABs Grab events, 2) how the HABs Grabs aligned with the seasonal blooms, 3) the total mass of MC in the western basin of Lake Erie, 4) the environmental parameters (i.e., nutrients, temperature) during the HABs Grabs, 5) comparison among biomass metrics, and 6) correlations between MCs, biomass, the MC-to-biomass ratio, and environmental parameters collected during the HABs Grab.

2. Materials and Methods

185 *2.1. Sample collection and handling methods*

186 The field and laboratory crews met at the University of Toledo Lake Erie Center several
187 days before the HABs Grab to calibrate water quality sondes (EXO2 YSI Inc., Yellow Springs,
188 OH, USA), distribute sample equipment and bottles, and demonstrate sample collection and
189 handling methods. This ensured that all samples were collected with the same methods. The
190 laboratory was set up to facilitate sample processing (filtering and dispensing aliquots).

191 During six hours on 9 August 2018, four institutions (Ohio State University [OSU] Stone
192 Laboratory, University of Toledo Lake Erie Center [UT-LEC], Bowling Green State University
193 [BGSU], and LimnoTech) collected a total of 100 samples in the U.S. waters of the western
194 basin of Lake Erie. The NOAA Lake Erie Harmful Algal Bloom Bulletin was used to determine
195 sample locations in advance of the field operation. On 7 August 2019, eight institutions and
196 agencies (the aforementioned, NOAA's Great Lakes Environmental Research Laboratory
197 [GLERL], Environmental and Climate Change Canada [ECCC], Fisheries and Oceans Canada,
198 and University of Windsor's Great Lakes Institute for Environmental Research [GLIER])
199 collected a total of 172 samples across the entire western basin, with sample locations pre-
200 determined in a grid-style pattern. Four research vessels were used in 2018, and eight were used
201 in 2019. The vessels sampled areas of the lake in proximity to their marina. In both years,
202 samples were collected between 8:00 AM and 2:00 PM local time to minimize variability caused
203 by the bloom movement (by advection and vertical migration) during sampling.

204 The same grab sample collection and handling methods were used both years and among
205 all groups. The vessels did not anchor at each site thus facilitating rapid sampling in order to
206 collect the high number of sampling stations per vessel targeted during the six-hour sampling
207 window. Upon arriving at the location, time, GPS, and water depth were recorded. Sample

208 equipment and bottles were first rinsed with lake surface water. A two-meter-long tube sampler
209 was used to collect an integrated water sample from the surface to 2 meters depth, and the water
210 was deposited into a clean and pre-rinsed 20-L bucket (Golnick et al., 2016). Lake water from
211 the bucket was poured into transparent 2.4-L polyethylene terephthalate glycol (PETG) bottles
212 and stored in a dark cooler while being transported back to the laboratory. No on-vessel
213 processing of the water took place. Water was poured into the calibration cup of an EXO2 sonde
214 (YSI Inc., Yellow Springs, OH, USA) immediately after sampling to record field parameters
215 (water temperature, pH, specific conductivity, turbidity, and chlorophyll and phycocyanin
216 fluorescence as relative fluorescence units (RFU)). After the water was collected, the vessel
217 moved to the next location, usually within 5 to 10 minutes after arriving.
218 All samples collected in the US waters were transported to the UT-LEC, whereas all
219 Canadian samples were transported to GLIER for processing. Both laboratories used the same
220 methods and supplies. Upon arriving at the processing laboratory, the sample bottles were
221 vigorously inverted several times, and aliquots were distributed for different parameters,
222 including filtration before sample splitting for some parameters.
223
224 *2.2. Laboratory analytical methods*
225
226 *2.2.1. Microcystins*
227 Every sample was analyzed for microcystins (MCs) with two analytical methods, and the
228 sample water for both methods came from the same aliquot. For total MCs, 25 mL was poured
229 into 60-mL amber glass vials and frozen at -20°C. All MCs samples were transported to OSU for
230 three freeze/thaw cycles to lyse cells, and following the third thaw, water was filtered into two

separate glass vials with glass microfiber (GMF, 0.45 µm) syringe filter to remove cellular debris. One vial was delivered to the City of Toledo Collins Park Water Treatment Plant for analysis of MCs by enzyme-linked immunosorbent assay (ELISA) and the second to the Lumigen Instrument Center at Wayne State University for analysis of 12 MC congeners and Nodularin by liquid chromatography with tandem mass spectrometry (LC-MS/MS). Extracellular MCs were analyzed similarly, albeit using water filtered the day of collection without freeze/thaw lysis.

MCs by ELISA were quantified with Abraxis kits (#520011; Eurofins Abraxis, Warminster, PA, USA) on an Abraxis Cyanotoxin Automated Assay System at the Toledo Water Treatment Plant. Samples that exceeded 4 µg/L were diluted and reanalyzed, and samples with analytical duplicates that differed by more than 10% were reanalyzed (Ohio Environmental Protection Agency, 2018).

Quantitative analysis of MCs by LC-MS/MS was conducted using an online concentration method (Birbeck et al., 2019). Briefly, using a Thermo Scientific TSQ Altis™ triple quadrupole mass spectrometer (Thermo Scientific, Waltham, MA, USA) with an EQuan MAX Plus™ system, 1 mL of sample was injected onto a loading column (Thermo Scientific Hypersil GOLD aQ 2.1 × 20 mm, 12 µm particle size) using an HTC PAL autosampler (CTC Analytics, Zwingen, Switzerland). The analytical column used was a Thermo Accucore aQ, 50 × 2.1 mm, 2.6 µm particle size column, kept at a stable temperature of 35°C for gradient analysis. Mass spectrometry analysis was performed using positive electrospray ionization source (ESI) mode. Quantitation data results were accomplished using TraceFinder™ EFS 4.1. The congeners analyzed for included MC-LR, RR, YR, WR, HtyR, HilR, [D-Asp^3]-RR, [D-Asp^3]-LR, LA, LF, LY, and LW, as well as nodularin. The MCs were purchased from Enzo Life Sciences, Inc.

254 (Farmingdale, NY, USA). The surrogate C_2D_5 MC-LR was purchased from Cambridge Isotope
255 Laboratories, Inc. (Tewksbury, MA, USA). It is noteworthy that [d-Asp^3] MC-RR has been
256 reported misidentified and has been a putative identification as [d-Asp^3, Dhb] MC-RR (Birbeck
257 et al., 2019).
258
259 *2.2.2. Nutrients*
260 A 100-mL aliquot was filtered to measure dissolved nutrients (nitrate, nitrite, ammonium,
261 dissolved reactive phosphorus, and dissolved reactive silicate) directly upon return to the lab.
262 First, two ~10-mL sub-aliquots were filtered through a 0.45-µm membrane filter to rinse the
263 equipment, with the remainder filtered and poured into a 60-mL PETG bottle, which was frozen
264 until analyzed. A sub-sample was taken for extracellular MCs. Unfiltered aliquots for total
265 phosphorus (TP) and total Kjeldahl nitrogen (TKN) were poured directly from the 2.4-L bottle
266 into separate 250 mL bottles and frozen at -20°C until analysis. Total N concentration was
267 calculated by the sum of nitrate, nitrite, and TKN. All nutrient samples were transported to OSU
268 for analysis following standard procedures (Chaffin et al., 2019).
269
270 *2.2.3. Chlorophyll and phycocyanin*
271 For chlorophyll (chl) *a* concentration, 50 to 100 mL, depending on phytoplankton
272 biomass, was filtered onto a 25 mm glass fiber filter (GF/F; 07 µm nominal pore size), noting the
273 volume. The filters were stored on silica gel in mini-Petri dishes at -80°C. Chl *a* was extracted
274 from the filters using dimethylformamide (DMF) and quantified by fluorometry (Golnick et al.,
275 2016). Additionally, samples were analyzed on the day of collection by a FluoroProbe (bbe
276 Moldaenke, GmbH) with a benchtop cuvette reader for chl *a* associated with four phytoplankton

277 groups: 1) green algae, 2) phycocyanin-rich cyanobacteria, 3) diatoms, chrysophytes and
278 dinoflagellates, 4) cryptophytes and phycoerythrin-rich cyanobacteria (Beutler et al., 2002;
279 Chaffin et al. 2013). The ratio between the FluoroProbe total chl *a* concentrations and the DMF
280 chl *a* concentrations was used to adjust the chl *a* concentrations attributed to each algal group
281 (Bridgeman et al., 2012). The Canadian samples from the 2019 event (n = 60) were not analyzed
282 with a FluoroProbe because the instrument was available at the time of the event.
283 Because the Canadian samples were not analyzed with a FluoroProbe, cyanobacteria-chl
284 *a* concentration was estimated using step-wise regression with the U.S. data. Input parameters
285 were DMF-chl *a*, total ELISA MCs, *mcyE*, and phycocyanin concentration. There was a very
286 tight relationship between DMF-chl *a* and cyanobacteria-chl *a* ($P < 0.001$ $R^2 = 0.974$), and no
287 other variables were included ($P > 0.05$). FluoroProbe cyanobacteria-chl *a* concentration for the
288 Canadian samples was therefore estimated using the equation:
289
290 Eq. 1 $FLP_{cyano} = (0.5926 * DMF_{chla}) + 0.0935$
291
292 Where FLP_{cyano} is the FluoroProbe cyanobacteria-chl *a* concentration (µg/L) and DMF_{chla} is the
293 chl *a* concentration (µg/L) measured from the DMF method.
294 For phycocyanin and phycoerythrin concentration, 400 mL was filtered onto a 47 mm
295 GF/C (1.2 µm nominal pore size) filter and immediately frozen at -80°C until extraction and
296 analysis. Extraction of the two pigments was done using 3 mL of 50 mM potassium phosphate
297 buffer (pH 6.7) at -4°C for 24 h and subsequently placed at +4°C for another 24 h. The extract
298 was centrifuged (20 min, +5°C, 3,210 × *g*, Beckman GS-6R rotor, Beckman Coulter Life
299 Sciences, Indianapolis, IN, USA) to remove the filter and cell debris. Analyses of phycocyanin

and phycoerythrin pigments were carried out according to Sarada et al. (1999) and Thoisen et al. (2017), respectively. Briefly, the supernatant's absorbance was measured at 455, 564, 592, and 750 nm on a USB2000 spectrophotometer (Ocean Optics, Dunedin, FL, USA) using potassium phosphate buffer as a blank. The absorbance values were scatter-corrected by subtracting the absorbance at 750 nm. The entire process was conducted under red light to avoid pigment degradation due to exposure to ambient light.

2.2.4. Molecular samples

DNA was extracted from 25 mm 1.2 µm pore size filters (Pall Versapor® acrylic copolymer; p/n 66393; Port Washington, NY, USA) using a Qiagen DNeasy® Blood and Tissue Kit (Qiagen, Germantown, MD, USA). Briefly, samples were incubated with 100 µL Qiagen ATL tissue lysis buffer, 300 µL Qiagen AL lysis buffer, and 30 µL proteinase K at 56ºC for 1 h with agitation, followed by vortexing at maximum speed for 10 minutes. Lysates were homogenized with a QiaShredder™ spin-column before purification, according to the DNeasy® protocol. DNA quantity and quality were assessed using a NanoDrop spectrophotometer (Thermo Fisher Scientific, NanoDrop Products, Wilmington, DE, USA). Genes indicative of the genetic potential to produce microcystins/ nodularin (*mcyE*), saxitoxins (*sxtA*) and cylindrospermopsins (*cyrA*) were enumerated using a commercially available multiplex qPCR kit (Phytoxigene CyanoDTec™ Toxin Genes Test; Diagnostic Technology, Sydney, Australia) modeled after the multiplex qPCR assay described elsewhere (Al-Tebrineh et al., 2012). The primers were general to all cyanobacteria and not targeted to a specific genus. Briefly, molecular grade water (80 µL) was added to each tube of a CyanoDTec™ cyanotoxin detection kit and processed following kit directions. A synthetic standard of known toxin gene copy (Diagnostic

Technology) was assayed in serial dilutions to generate a standard curve spanning five orders of magnitude (100-1,000,000 copies) for each target toxin gene. Amplification was conducted on a Quantabio Q Real-Time PCR system (Quantabio, Beverly, MA, USA) in a total volume of 25 μL. Each sample was run in duplicate. Gene copies in each reaction were calculated using the Quantabio Q software and back-calculated to copies mL^{-1}. Only the *mcyE* gene abundances will be reported in this study.

Random shotgun sequencing of the whole community was performed on 25 samples from the 9 August 2018 HABs Grab to estimate the proportion of the *Microcystis* population capable of producing MCs. These 25 sampling sites ranged from 14 km to 52 km away from the Maumee River's mouth. Metagenomic shotgun reads were subjected to the Geomicrobiology Quality Check protocol as part of the Metagenomics Pipeline, which can be found at https://github.com/Geo-omics/scripts. Briefly, reads were trimmed for quality and removal of Illumina adapters and spike-ins using BBDuk. Quality checked reads were then de-replicated and forward and reverse reads were pooled. The relative abundance of *Microcystis* was quantified with a Basic Local Alignment Search Tool (BLAST) v.2.8.1 search of reads against the v4 region of all *Microcystis* 16S rRNA genes in the SILVA database v. 138.1. To avoid counting non-specific matches (*i.e.*, from other cyanobacteria), the 16S v4 regions from all cyanobacteria deposited in the SILVA database v. 138.1 were included in the BLAST database as competitors for reads (Supplemental File 2). The relative abundance of *Microcystis mcyD* and *mcyE* genes was quantified with a BLAST search to all *Microcystis mcy* genes *D* and *E* genes publicly available in the IMG/MER database (https://img.jgi.doe.gov/). To avoid non-specific mapping, *mcy* genes from taxa other than *Microcystis* were also included in the BLAST database as competitors for reads (Supplemental File 3). Aligned reads were counted as positive matches if

346 they had 80% query coverage and 95% sequence identity. These cutoff parameters, database
347 metrics, and mapping tools were tested exhaustively to ensure specificity and sensitivity by
348 cross-checking matches to the full SILVA database and a custom universal database
349 (https://github.com/TealFurnholm/Meta-NGS_Reference_Database). Filtered reads per gene
350 were then quantified and normalized by the length of the gene and sequence library size. Counts
351 for ambiguous assignments (alignment to multiple subjects with identical bitscores) were divided
352 by the total number of subjects. Normalized read counts for the *mcy* gene were then divided by
353 normalized read counts for the *Microcystis* 16S rRNA gene (assuming one *mcy* and 16S rRNA
354 gene copy per cell) to give an estimate of the proportion of the *Microcystis* population within
355 each sample that contained each *mcy* gene within their genome.
356
357 *2.3. Data analysis*
358
359 *2.3.1. Water currents (FVCOM)*
360 The hydrodynamic conditions were simulated using the Lake Erie operational version of
361 the Finite Volume Community Ocean Model (FVCOM; Chen et al., 2003) maintained by
362 NOAA. FVCOM is a three-dimensional (3D), free-surface, primitive-equation model that solves
363 the integral form of the governing equations on an unstructured, sigma-coordinate mesh. The
364 advantage of an unstructured grid mesh for shoreline fitting and local mesh refinement makes the
365 model particularly attractive in applications to coastal waters. FVCOM has been applied in many
366 coastal systems characterized by geometric complexities and highly variable flow patterns,
367 including various applications to the Great Lakes (for example: Anderson et al., 2015; Rowe et
368 al., 2016; Xue et al., 2017).

369 The Lake Erie (LE)-FVCOM was configured with horizontal resolution ranging from 200
370 to 2500 m and 21 vertical terrain-following sigma layers. The inflow and outflow to the lake
371 include Detroit, Maumee, and Niagara Rivers. The LE-FVCOM was run in a hindcast mode for
372 the year 2018 and 2019 and driven by hourly meteorological surface forcing from the High-
373 Resolution Rapid Refresh (HRRR), a cloud-resolving and convection-allowing weather forecast
374 and data assimilation system running real-time at a 3-km grid resolution. The LE-FVCOM
375 utilized the Mellor and Yamada level 2.5 (MY-2.5) and Smagorinsky turbulent closure schemes
376 for vertical and horizontal mixing, respectively (Mellor and Yamada, 1982; Smagorinsky, 1963).
377
378 *2.3.2. Total microcystin mass*
379 Total MC mass was determined for each of the HABs Grab sampling events by applying
380 similar geospatial methods. Geolocated concentrations determined for the homogenized samples
381 from the upper 2 m of the water column at each sampling station by ELISA were used to
382 construct a geodatabase for each sampling event, along with existing bathymetric data rather than
383 field-reported water depths. Sampling station data were bounded by a set of points that was
384 developed by making conservative assumptions. Zero-concentration open lake boundary points
385 were created along the August 2018 bloom edge from the 9 August forecast bloom position
386 reported in the 6 August NOAA HABs Bulletin based on a 5 August satellite image. The entire
387 basin was sampled in the 9 August 2019 event, so the creation of a set of open-water boundary
388 points was not necessary. Shoreline point values were projected as constants from the nearest
389 offshore sampling station in both years, including for island shorelines as appropriate.
390 The entire MC dataset of sampling stations and constructed bounding values was
391 interpolated using inverse distance weighting (IDW) methods (Philip and Watson, 1982; Watson

392 and Philip, 1985) within the ArcMap 10.7.1 Spatial Analyst extension software package
393 (Environmental Systems Research Institute, Redlands, CA). The interpolated MC concentrations
394 were converted to 100-m by 100-m grid cells and multiplied by the average water depth in each
395 grid cell to determine a total mass of MC per grid cell for the whole water column. Masses were
396 then summed for all column grid cells to calculate a total MC mass for each sampling event.
397 Recent studies of the vertical distribution of biomass and MC in western Lake Erie have revealed
398 that significant cyanobacteria and toxin remain at depth, even on days when cyanobacterial
399 colonies are observed at the surface (Kramer, 2018). Surface and bottom MC concentrations
400 were also similar in weekly samples collected by NOAA GLERL during summer 2019
401 (Supplemental Fig. 1). Furthermore, the highest MC concentrations usually occur in the shallow
402 nearshore waters where the upper 2 m make up a larger proportion of the water column, whereas
403 MC concentrations are an order of magnitude less at deeper sites (Palagama et al., 2020). The
404 calculation assumed a uniform water column concentration for each grid cell. This assumption
405 may yield an overestimate of total MC mass if concentrations declined significantly between the
406 upper two meters of the water column and the deeper waters. However, other available data
407 collected around the HABs Grab dates do not indicate that the assumption of consistent top to
408 bottom MC concentrations is unreasonable, and it would be overly conservative to assume all
409 MCs were within the upper 2 m.
410
411 *2.3.3. Spatial Interpolations*
412 Spatial interpolations of the HABs Grab data were conducted in ArcGIS v10.3 with the
413 Kriging function. All default settings were used. The Kriging outputs were clipped to the area
414 sampled.

415

416 *2.3.4. Correlation among parameters*

417 A Pearson correlation coefficient (*r*) matrix was generated among metrics used to
418 estimate cyanobacterial biomass during the 9 August 2018 and 7 August 2019 HABs Grab. For
419 our analysis, we considered *r* values less than 0.30 to have a negligible correlation, 0.31 to 0.50
420 to be weakly correlated, 0.51 to 0.70 to be moderately correlated, 0.71 to 0.90 to be strongly
421 correlated, and 0.91 to 1.0 to be very strongly correlated. The parameters included those
422 measured aboard the research vessels with the YSI handheld units (chl and PC relative
423 fluorescence units), measured in the laboratory with the FluoroProbe (cyanobacteria-specific chl
424 *a* and total chl *a* concentrations), and filtered extracted chl *a*, PC, and cyanobacteria-specific 16S
425 gene copies. Total MCs and extracellular MCs measured by ELISA were also included in the
426 matrix to determine how toxin concentration correlated with the biomass metrics.

427 Scatter plots of MCs, total chl *a*, and the ratio of MCs to chl *a* against potential
428 environmental explanatory variables (for example, temperature, pH, nutrient concentrations) for
429 samples with MCs concentrations greater than 1 µg/L were generated to display correlations and
430 patterns visually. Additionally, residuals from the MC-ELISA vs. chl *a* regression equation were
431 calculated and plotted against environmental explanatory variables. IBM SPSS Statistics v23
432 were used for all data analysis.

433

434 *2.4. Seasonal progression of the Lake Erie bloom*

435 Routine monitoring (every ~10 days) data collected by the UT-LEC was used to put the
436 2018 and 2019 HABs Grab into the context of the seasonal bloom progression. Data from five
437 sites representative of the western basin, extending 14 to 31 km from the Maumee River's mouth

438 (Supplemental Fig. 2), were averaged for each sample date. The five sites selected have been
439 routinely monitored by UT-LEC since 2002, and *Microcystis* biovolume in this dataset aligns
440 well with remote sensing data (Bridgeman et al., 2012; 2013). Water samples were collected
441 throughout the water column and analyzed by a benchtop FluoroProbe, as described above, to
442 determine the relative contribution of green algae, cyanobacteria, diatoms, and cryptophytes to
443 total chl *a* concentration. ELISA was used to measure total MC concentrations.
444 Seasonal progression of the bloom spatial extent was documented by ECCC's
445 EOLakeWatch, using Sentinel-3 OLCI satellite imagery. In order to minimize cloud-related
446 uncertainties in image products, 14-day rolling average chl *a* maps were produced (Binding et
447 al., 2021). Bloom extent was delineated using the threshold of satellite-derived chl *a* > 10 µg/L.
448
449 **3. Results**
450 *3.1. Progression of the blooms*
451 Cyanobacteria-specific chl *a* concentrations increased from lows in June to peaks in late
452 July and early August and then decreased throughout August and September in both years (Fig.
453 1A & 1B). The August chl *a* peak of 2018 (7.9 ± 2.1 µg/L) was lower than that of 2019 (37.8 ±
454 9.7 µg/L). Total MCs followed a similar pattern as cyanobacteria chl *a* and peak MCs
455 concentrations in 2018 (2.2 ± 0.8 µg/L) were less than that of 2019 (5.5 ± 1.4 µg/L). The peak
456 bloom spatial extent in 2018 lasted from mid-August through mid-September, covering an area
457 of approximately 400 km^2 (Fig. 1C). In 2019, the bloom extent reached 1171 km^2 in mid-August,
458 declined slightly in late August, and peaked again during mid-September at 1310 km^2 (Fig. 1D).
459 Total chl *a* (determined by the DMF method) increased throughout summer during 2018,
460 peaking at 19.1 ± 3.4 µg/L in early September. Total chl *a* in 2019 was greater than 30 µg/L

461 from late July throughout early September, with the highest concentration on 1 August of 45.7 ±
462 11.5 µg/L (Fig. 1E and 1F). Pre-bloom of both years, diatoms accounted for more than 60% of
463 total chl *a*, and cyanobacteria made up a relatively low percentage of total chl *a* (< 25%).
464 Cyanobacteria accounted for 52% of the chl *a* during the peak bloom in 2018, but in the larger
465 bloom year of 2019, cyanobacteria accounted for 81%. Diatoms returned to dominance following
466 the cyanobacterial bloom peak in both years. These data indicate that both HABs Grab events
467 were conducted during the peak bloom conditions for biomass, bloom extent, MC
468 concentrations, and cyanobacterial dominance of the phytoplankton community.
469
470 *3.2. Spatial data of biomass and microcystins*
471 During the 9 August 2018 HABs Grab, the highest concentrations of chl *a* (measured
472 with the DMF method) occurred within several kilometers from the Ohio and Michigan
473 shorelines, and lower concentrations were measured in the center of the basin (Fig. 2). All 2018
474 samples had a filter-extracted chl *a* concentration less than 21 µg/L, except the sample closest to
475 the Maumee River, which had 54.3 µg/L and the FluoroProbe determined 61% of the chl *a* was
476 from green algae and diatoms. Much higher chl *a* concentrations, nearly an order of magnitude
477 greater, were measured on 7 August 2019 (Fig. 2). The highest concentrations occurred in
478 Maumee Bay near the mouth of the Maumee River (> 150 µg/L), and concentrations decreased
479 with increasing distance from Maumee Bay. There was a 'finger' of higher chl *a* concentrations
480 that extended northward in the center of the basin into Ontario waters. Cyanobacteria-specific chl
481 *a* measured by the FluoroProbe showed nearly identical spatial pattern as the DMF method
482 (Supplemental Fig. 3).

483 Microcystins (measured by ELISA) during 9 August 2018 were highest along the Ohio
484 shoreline and around the Bass Islands on the eastern edge of the western basin ranging from 2 to
485 5 µg/L (Fig. 2), and MCs concentrations were lower in the center of the basin. In the 7 August
486 2019 HABs Grab the highest MCs concentrations, 15 to 50 µg/L, were measured in Maumee
487 Bay (western corner of the basin) and decreased with distance from Maumee Bay. Microcystins
488 were below detection (<0.3 µg/L) in the northwest portion of the basin where the Detroit River
489 outflows into Lake Erie and below detection around the Bass Islands. Likewise, there was a
490 'finger' of MCs ranging from 1 to 5 µg/L in the center of the basin, reaching into Ontario waters.
491 The ratio of total MC to chlorophyll concentrations (MC:chl *a*) was not consistent across
492 the basin, and the spatial pattern was not the same between years. On 9 August 2018 HABs Grab
493 there were 'hot spots' with MC:chl *a* ratios greater than 0.20 in the south-center portion of the
494 basin and around the islands (Fig. 2). Lower ratios were recorded in Maumee Bay and the
495 northern half of the basin. On the 7 August 2019 HABs Grab, the majority of the western basin
496 had MC:chl *a* ratios less than 0.15, and hot spots greater than 0.20 were confined to within ~10
497 km from the Ohio shoreline and within the 'finger' of higher biomass extended northward in the
498 center of the basin (Fig. 2).
499 Percent of the *Microcystis* population capable of producing MCs ranged from 15.8 % to
500 34.0%, and the overall average was 21.9% (Fig. 3). Both MC genes, *mcyD* and *mcyE*, gave very
501 similar results (Fig. 3). Nineteen of the 25 samples were less than 25%. The percent toxigenic
502 *Microcystis* did not correlate with distance from the Maumee River or with any environmental
503 parameter measured. Overall, this indicated that less than one-quarter of the *Microcystis* cells
504 during the 9 August 2018 HABs Grab were capable of producing MCs.
505

3.3. Water currents

Simulations show that daily average circulations in the surface mixed layer on both HABs Grab days were characterized by a general pattern of west-to-east flow exiting the basin (Michalak et al., 2013; Schwab et al., 2009). Detailed flow patterns reveal how the spatial variability of the observed blooms was influenced by hydrodynamic transport. Stronger flow occurred during the 9 August 2018 HABs Grab (Fig. 4A). The water mass associated with the Detroit River flowed southward and could reach the central part (41.7 °N – 41.8 °N) of the basin before turning eastward and exiting through the north and middle channels divided by Pelee Island. Accordingly, the water mass and cyanobacteria associated with the Maumee River were compressed around the west coast out of Maumee Bay and moved along the southern part of the basin.

During the 7 August 2019 HABs Grab, the circulation was weaker, which led to less eastward hydrodynamic transport of the cyanoHAB and allowed for longer residence time in the basin (Fig. 4B). The majority of Detroit River water was more constrained to the northern part of the basin with an anti-clockwise turn to the northeast to exit through the north channel. Correspondingly, the weakened southward intrusion allowed the water mass and cyanoHAB associated with the Maumee River to extend further north, compared to the bloom pattern during the 9 August 2018 HABs Grab. The bloom was distributed mostly in the southern and central parts of the basin. A portion of the bloom was mixed into the anti-clockwise circulation in the northern part of the basin described above, leaving a ‘finger’ of bloom biomass pointing towards Canada and Pigeon Bay.

3.4. Nutrient concentrations

529 Except for dissolved inorganic N (DIN), higher concentrations of nutrients were observed
530 on 7 August 2019 (Fig. 5). DIN concentrations on 9 August 2018 ranged from 40 to 60 µmol/L
531 in Maumee Bay, and concentrations near the Michigan and Ohio shorelines (20 – 40 µmol/L)
532 were greater than the center of the basin (15-20 µmol/L). On 7 August 2019, DIN concentrations
533 were highest near Little Cedar Point (20 – 40 µmol/L) and were less than 20 µmol/L in the
534 majority of the western basin. The lowest DIN concentrations (5-10 µmol/L) were recorded in
535 the center of the basin within the 'finger' of biomass extending into Ontario waters. Nitrate made
536 up the majority of the measured DIN. Ammonium concentrations on 9 August 2018 were less
537 than 2 µmol/L nearshore and less than 1 µmol/L in the center of the basin. On 7 August 2019,
538 ammonium concentrations between 6 and 8 µmol/L were measured in Maumee Bay, and
539 concentrations decreased with increasing distance from Maumee Bay.
540 Total N concentrations (the sum of nitrate, nitrite, and TKN) in 9 August 2018 followed
541 the same spatial pattern as DIN concentrations. Total N in 7 August 2019 was greatest in
542 Maumee Bay (150 – 275 µmol/L) where the highest levels of cyanoHAB biomass occurred, and
543 TN concentrations were lower (25 - 50 µmol/L) in the rest of the basin.
544 In both years, total P concentrations were greatest in Maumee Bay and decreased with
545 increasing distance from the bay. Total P concentrations were greater during 7 August 2019 in
546 Maumee Bay and the rest of the basin. Dissolved reactive P concentrations were less than 0.1
547 µmol/L in most samples in both years and often below detectable levels (<0.03 µmol/L).
548 The ratio of total N to total P concentrations (TN:TP) exceeded 30 (by moles) during
549 both HABs Grabs. On the 9 August 2018 HABs Grab, TN:TP was between 75 and 100 for most
550 of the area sampled. On 7 August 2019, most of the southern half of the basin had TN:TP

between 50 and 125, whereas the northern half of the basin had much higher TN:TP of 150 to 520. The higher TN:TP in the northern half of the basin was due to lower TP concentrations.

3.5. Total MC mass and average concentration

The total mass of MCs (measured by ELISA) in the western basin on 7 August 2018 was estimated as 11,513 kg, and the total mass on 9 August 2019 was estimated as 30,691 kg (Table 1). The MC mass estimated assumed the MC concentration measured in the 0-2 meter sample was representative of the unsampled water deeper than 2 meters (see methods). The average MC concentration in samples with detectable MCs (> 0.30 µg/L) was 1.94 µg/L and 5.02 µg/L on the 2018 and 2019 HABs Grabs, respectively. The approximate area of the western basin is 2780 km^2 and the approximate mean depth is 8 meters, which gives a volume of 2.224×10^{10} m^3. The basin-wide average MC concentration would have been 0.52 µg/L and 1.38 µg/L on 9 August 2018 and 7 August 2019, respectively, if the cyanoHAB was evenly spread out throughout the basin.

3.6. Metrics comparison and correlations to microcystins

One sample on 9 August 2018 that was collected near the mouth of the Maumee River was removed from the correlation matrix because it had chl values two to three times greater than the second-highest sample (depending on metric) due to high levels of green algae and diatoms. Nearly all cyanobacterial biomass metrics significantly ($p < 0.05$) correlated with each other, but more importantly, *r* values (strength of correlation) ranged from 0.43 (very weak correlation) to 0.99 (very strongly correlated), and correlation coefficients often differed between years within a parameter (Table 2). For this section, only the *r* values greater than 0.70 are

highlighted (strongly correlated). The handheld YSI chl RFU strongly correlated with 2018 PC RFU and with 2018 FluoroProbe total chl *a*, but no correlations in 2019 had a *r* value greater than 0.70. It is important to note that 2018 had greater chl RFU values, but lower filter-extracted chl *a* concentrations than 2019. Phycocyanin RFU strongly correlated with 2019 FluoroProbe cyanobacteria-chl *a*, FluoroProbe total chl *a* in both years, and with 2019 filter-extracted chl *a*. Of special note, chl RFU and PC RFU did not strongly correlate with their respective traditional laboratory methods. The FluoroProbe-estimated cyanobacteria-specific chl *a* very strongly correlated with FluoroProbe total chl *a* and filter-extracted chl *a* and, in 2019 only, with cyanobacteria 16S gene copies, PC RFU, and *mcyE* gene copies. The FluoroProbe-estimated total chl *a* concentrations were strongly correlated with filter-extracted chl *a* ($r = 0.90$ and 0.98), and with cyanobacteria-specific, PC RFU, and 2019 chl RFU. Filter-extracted-chl *a* concentrations were very strongly correlated with both FluoroProbe parameters and cyanobacterial 16S gene copies, and strongly correlated with 2019 PC RFU and 2019 *mcyE* gene copies. Filter-extracted-PC concentrations did not strongly correlate with any parameter. Cyanobacterial 16S gene copies very strongly correlated with both FluoroProbe parameters, filter-extracted chl *a*, and *mcyE* gene copies. Gene copies of *mcyE* measured during 2019 strongly correlated with both FluoroProbe parameters and filtered-extracted chl *a*, but *mcyE* did not correlate with any parameter in 2018.

On 9 August 2018 total MCs concentrations measured with the ELISA method correlated with cyanobacteria-chl *a* and chl *a* extracted from a filter. On 7 August 2019 MCs strongly correlated with every biomass metric to some degree ($r > 0.71$) except for filter-extracted PC, and 2019 MCs were very strongly correlated with cyanobacteria-specific chl *a* , FluoroProbe

596 total chl *a*, and filter-extracted chl *a* (r = 0.90 – 0.92). Extracellular MCs concentrations
597 correlated only with cyanobacterial 16S gene copies.
598 Total MCs measured by ELISA ranged from less than detectable levels (< 0.15) to 46.56
599 µg/L, whereas the LC-MS/MS sum of 12 congeners ranged from 0.01 to 26.53 µg/L (Fig. 6). In
600 both years, the four MC congeners found in the highest concentrations were MC-LR (44.4%,
601 35.9% in 2018, 2019, respectively), RR (23.1%, 33.6%), LA (16.7%, 13.5%), and YR (13.6%,
602 15.7%), and the other congeners analyzed for were collectively usually less than 3%
603 (Supplemental Fig. 4). Despite the differences in concentrations, the two methods were highly
604 correlated. Linear regressions conducted separately for each year gave similar slopes (0.5125 for
605 2018 and 0.5462 for 2019), and the R^2 was 0.79 for 2018 and 0.95 for 2019. This indicates that
606 MCs concentrations measured by ELISA were approximately twice as high as measured by LC-
607 MS/MS.
608
609 *3.7. HAB biomass and MC correlations with environmental parameters*
610 Filter-extracted chl *a* concentrations were selected for comparison with the environmental
611 parameters due to the high degree of correlation with the other cyanobacterial biomass metrics
612 (Table 2). Cyanobacteria-specific chl *a* measured with the FluoroProbe could have been
613 displayed here, which gave very similar patterns as total chl *a*, but we chose total chl *a* owing to
614 the greater number of samples, and FluoroProbe data are less common than filter-extracted chl *a*.
615 Cyanobacteria-specific chl *a* metrics are displayed in the supplemental document.
616 MCs increased with filter-extracted chl *a* concentration on 7 August 2019 but not 9
617 August 2018 (Fig. 7A); however, in 2018 MCs did increase with cyanobacteria-chl *a*
618 (Supplemental Fig. 5). The ratio of MCs to chl *a* (MC:Chl *a*) ranged from near 0 (MCs lower

than detection) to 0.31 for all samples but three (Fig. 7b). On 9 August 2018, there was no relationship between MC:Chl *a* and cyanoHAB biomass (as chl *a* concentration). On 7 August 2019, the minimum MC:Chl *a* increased with increasing chl *a* concentration. For example, MC:Chl *a* ranged from 0 to 0.3 for chl *a* concentration less than 10 µg/L, but MC:Chl *a* ranged from 0.15 to 0.3 for chl *a* concentrations greater than 50 µg/L. Regarding the MCs to cyanobacteria-specific chl *a* ratio (MC:cyanobacteria-chl *a*), 7 August 2019 was very similar to MC:Chl *a* because cyanobacteria were the majority of the chlorophyll (Supplemental Fig.5). However, on 9 August 2018, most samples had a MC:cyanobacteria-chl *a* between 0.1 and 0.6, but MC:Chl *a* ranged from near 0 to 0.3. Green algae and diatoms were in relatively greater concentrations during the 2018 HABs Grab, and their contribution to total chl *a* decreased MC:Chl *a*.

The correlations between MCs and chl *a* concentration with environmental parameters showed similar patterns (Figs. 8 and 9), which was due to the high correlation between MCs and chl *a* (Table 2). The highest MCs and chl *a* concentrations were recorded in lake water temperatures between 25ºC and 27ºC (Fig. 8). Higher pH values were observed on 7 August 2019 than 9 August 2018, and on 7 August 2019 highest MCs and chl *a* concentrations occurred at pH greater than 9.0, but low concentrations of both MCs and chl *a* were also observed at high pH values. MCs and chl *a* increased with turbidity, but this pattern was expected because algal biomass is captured in turbidity measurements. On 7 August 2019, the highest concentrations of MCs and chl *a* concentrations occurred at specific conductivity between 270 and 320 µS/cm, which reflects water closest to the Maumee River's mouth. The toxin-to-biomass ratio, MC:Chl *a*, did not correlate with temperature, turbidity, pH, or specific conductivity. The residuals

641 between MC vs. chl *a* were centered around 0 throughout the range of the observed physical
642 parameter, indicating no relationship.

643 Regarding nutrients, MCs and chl *a* concentrations increased linearly with TKN, TN, and
644 TP concentrations (Fig. 9). MCs measured on 7 August 2019 also increased with DIN, but that
645 pattern was not observed on 9 August 2018. The highest concentrations of MCs and chl *a*
646 concentrations occurred at TN:TP concentration ratios between 50 and 100 (molar). The MC:chl
647 *a* did not correlate with any N or P parameter during 9 August 2018. On 7 August 2019, the
648 majority of lower toxin-to-biomass ratios (MC:chl *a* < 0.2) occurred at low DIN (< 20 µmol/L)
649 and low TP (< 1 µmol/L) concentrations, and higher concentrations had greater MC:chl *a*. For
650 TKN concentrations less than 75 µmol/L, MC:chl *a* ranged from 0.05 to 0.4, but MC:chl *a*
651 increased with increasing TKN concentrations greater than 75 µmol/L. The residuals between
652 MC vs. chl *a* were centered around 0 across the range of TKN, TN, TP, and TN:TP. The
653 residuals increased with DIN concentration on 7 August 2019 ($R^2 = 0.32$). The regression line
654 crossed the DIN axis at 17.9 µmol/L, which indicates samples collected from waters with DIN
655 concentrations less than 17.9 µmol/L had less MC per chl *a* compared to samples collected from
656 higher DIN concentrations.
657

658 **4. Discussion**

659 *4.1. Comparison to other years*

660 The tremendous inter-annual variation of cyanoHAB biomass in Lake Erie is primarily
661 driven by springtime (March-July) P load from the Maumee River (Stumpf et al., 2016b), and
662 cyanoHAB biomass in 2018 and 2019 followed the expected pattern. Much higher biomass was
663 recorded during 2019 than in 2018 (Fig. 1), which corresponded to heavy springtime rainfall and

664 nutrient loading. Despite the difference in annual cyanoHAB biomass, temporal patterns are
665 usually consistent from year to year, with cyanobacteria first appearing in Maumee Bay during
666 July, peaking between mid-August to early September, and decreasing throughout the autumn
667 (Binding et al., 2021; Bridgeman et al., 2013; Stumpf et al., 2016b), although the very large 2011
668 bloom peaked in mid-October (Binding et al., 2012; Stumpf et al., 2012). Overall, the
669 cyanoHABs during 2018 and 2019 were typical blooms and followed the expected patterns
670 based on previous years. Furthermore, the 2018 and 2019 HABs Grabs occurred during the peak
671 biomass of each year.

672 Analysis of random shotgun sequencing data and quantification of the microcystin-
673 producing (*mcy*) gene and *Microcystis* 16S rRNA genes showed that, on average, only 22.6%
674 and 21.1% of the *Microcystis* cells (based on *mcyD* and *mcyE*, respectively) present during the 9
675 August 2018 HABs Grab had the potential to produce MCs (Fig. 3). There was close agreement
676 between data from *mcyD* and *mcyE*, supporting the precision of the method. The percentage of
677 potential MC-producers was not related to distance from the Maumee River, which agrees with
678 previous studies that the *Microcystis* populations in the river are separate from those in the lake
679 (Kutovaya et al., 2012). The percentage of MC-producers could have looked different if we
680 conducted the HABs Grab earlier or later during the bloom's progression. Potential MC-
681 producers inoculate the water column sooner than non-MC-producing strains (Kitchens et al.,
682 2018), which suggests the percentage of potential MC-producers could have been higher if we
683 sampled earlier in the bloom. However, the percentage of potential MC-producers could have
684 been lower later in the bloom when N and light become limiting (Chaffin et al., 2013), and the
685 competitive balance between MC-producing and non-MC-producing strains is shifted towards
686 the latter strains (Davis et al., 2010; Kardinaal et al., 2007). Furthermore, N-limitation and the

687 shift to non-MC-producing strains manifests in lower MC to biomass ratios in late summer and
688 fall (Gobler et al., 2016; Horst et al., 2014).
689
690 *4.2. Microcystin mass notes*
691 The HABs Grabs surveys allowed us to estimate, with reasonably high confidence,
692 11,513 kg and 30,691 kg of MCs in the western basin on a single day during peak cyanoHAB
693 conditions on 9 August 2018 and 7 August 2019, respectively. The uncertainty associated with
694 these estimates would be higher with fewer samples due to the spatial heterogeneity of biomass
695 and MC concentrations. The cyanoHAB bloom boundary is particularly problematic for these
696 estimates. For example, in the northwest portion of the 7 August 2019 cyanoHAB (Michigan
697 shore), only 5 km separated high biomass (chl *a* > 50 µg/L) and high MCs (> 5 µg/L) from low
698 biomass (chl *a* < 5 µg/L) and MC below detection (< 0.3 µg/L). A rapid gradient was observed in
699 Maumee Bay between the highest biomasses and MC concentrations and intermediate levels
700 over a similarly short distance. Without the high number of samples with high spatial resolution,
701 we would have missed these cyanoHAB edge gradients and would have had lower-confidence in
702 MC total mass estimates. The strong spatial gradients in cyanoHAB biomass and MCs and the
703 potential for missing fine-scale variability with discrete sampling further demonstrate the value
704 of synoptic high-resolution satellite observations in capturing these dynamic events.
705 The revelation of tons of MCs in the western basin from the HABs Grab events can be
706 alarming, especially to managers and the general public, without the proper context. The high
707 mass of MCs not only reflects bloom expanse but also reflects the large area (~2780 km^2), and
708 hence large volume, of the western basin. Total mass estimates are useful for researchers
709 studying cyanoHAB toxin dynamics and the relationships to environmental triggers on an

ecosystem scale. However, local MC concentrations are more important for managers and the public because concentrations are associated with human health risks. For example, if the cyanobacterial biomass and MCs were spread throughout the basin by stronger currents, the basin-wide MC concentration would have been 0.52 µg/L or 1.38 µg/L, on 9 August 2018 and 7 August 2019, respectively. It is critically essential to message these results in the proper context.

4.3. Microcystin to biomass ratio

The HABs Grab dataset is the largest single-day characterization of the Lake Erie cyanobacteria-dominated blooms. While there have been previous studies in Lake Erie that presented relationships between MC and cyanobacterial biomass with environmental parameters, those studies grouped data collected from a few sites and throughout the growing season (Horst et al., 2014; Millie et al., 2009; Rinta-Kanto et al., 2009; Wang et al., 2009). Studies that group data from many dates overlook how the relationship between two parameters may change throughout the seasons, which may skew trends and result in larger uncertainty. The relationships presented here from the one-day surveys omit the temporal impacts among parameters; however, these relationships would likely be different if the HABs Grabs were conducted later in the year when P and N become co-limiting to cyanobacterial growth and MC production, and there is a shift towards non-MC-producing strains (Gobler et al., 2016).

Recently, Liu et al. (2020) used the MC:chl *a* ratio to hindcast MC concentrations from satellite-derived chl *a* concentrations for Lake Erie 2009 – 2016. Liu et al. (2020) stated that MC:chl *a* varied more temporally than spatially; however, our HABs Grab surveys showed that MC:chl *a* was not consistent spatially. MC:chl *a* ranged from 0.06 to 0.32 across the entire western basin during both HABs Grabs when MC were detected at concentrations greater than

733 1.0 µg/L, a range that is comparable to the seasonal variability of MC:Chl *a* documented in Liu
734 et al. (2020). Furthermore, waters within a few kilometers of the Ohio shoreline, which serve as
735 sources of drinking water for several municipalities, had the highest MC:chl *a* ratios. Thus,
736 forecasting MC concentrations based on chl *a* concentrations and an assumed constant MC:chl *a*
737 ratio could result in modeled MC concentrations that are off by a factor of up to 5.3 during the
738 early stages of the peak bloom.

739 During the large bloom year of 2019, the MC:chl *a* ratio did appear to have some
740 dependency on cyanobacteria biomass (as measured by chl *a*). As biomass increased, so did the
741 minimum MC:chl *a* per chl *a* concentration. For example, at chl *a* concentrations of 25 µg/L,
742 MC:chl *a* ranged from 0.05 to 0.30, but at chl *a* concentrations from 50 to 200 µg/L, MC:chl *a*
743 ranged from 0.15 to 0.30. Thus, high cyanobacterial biomasses were more likely to be associated
744 with higher MC concentrations that would warrant a recreational contact advisory. Nevertheless,
745 lower biomasses may also warrant the advisories if the MC:chl *a* is on the high side of the range.
746 For example, the range of predicted MC concentrations for chl *a* concentrations of 25 µg/L and
747 50 µg/L would be 1.25 to 7.5 µg/L and 7.5 to 15 µg/L, respectively. In the state of Ohio,
748 recreational advisories are posted for MC concentrations exceeding 6 µg/L. The uncertainty
749 associated with MC:chl *a* at chl *a* concentration of 25 µg/L would give predicted MC
750 concentrations both above and below Ohio's recreational guideline, but a higher chl *a*
751 concentration of 50 µg/L would exceed Ohio's recreation guideline under the entire MC:chl *a*
752 range observed in this study. In terms of drinking water treatment, the large uncertainty in
753 MC:chl *a* makes it difficult for water treatment plant operators to estimate MC concentrations for
754 the optimization of treatment. If managers estimate MC exposure risk from models based on
755 MC:chl and chl *a* concentrations, it would be wise to take a more conservative approach and

assume the high range of projected MC concentrations. The difficulty in estimating MC concentration from chl *a* highlights the need for rapid MC tests and a better understanding of the factors that regulate MC production.

Several environmental parameters were investigated as explanatory variables for the relationships between MC and chl *a* observed during our HABs Grab. The data collected on 9 August 2018, the low HAB biomass year, did not show any patterns or correlations, likely due to the high range of MC:chl *a* observed at low biomasses (as discussed above). On 7 August 2019, MC:chl *a* showed a negligible relationship with total P ($R^2 = 0.10$), which the tautologous relationship between chl *a* and total P could explain this trend. MC:chl *a* and the residuals of MC vs. chl *a* showed better relationships with DIN ($R^2 = 0.18, 0.32$, respectively). The lowest within-bloom MC:chl *a* ratios occurred in the center of the basin (Fig. 2) where the DIN concentrations were less than 10 µmol/L (Fig. 5), which is known to constrain MC production in *Microcystis* dominated blooms (Chaffin et al., 2018a; Gobler et al., 2016). Moreover, the residuals from the MC vs. chl *a* plot showed less than expected MCs at similar DIN concentrations, further supporting N-limitation of MC synthesis (Fig. 9). So even at these larger spatial scales, these results were consistent with the prediction by the theory of ecological stoichiometry of phytoplankton toxins, which links the production of the N-rich MCs by cyanobacteria to N availability (Brandenburg et al., 2020; Van de Waal et al., 2014; Wagner et al., 2019). Furthermore, MC:chl *a* has been shown to decrease throughout the season (Chaffin et al., 2018b; Horst et al., 2014; Liu et al., 2020), and the decrease of MC:chl *a* paralleled drawdown of DIN concentrations (Chaffin et al., 2018b; Horst et al., 2014). Nitrate concentration data, or knowledge of how nitrate concentration changes throughout the season, could improve MC concentration predictions based on HAB biomass and the MC:chl *a* ratio. Ammonium is often in

779 low concentrations during cyanobacterial blooms (< 1 µmol/L) because uptake rates exceed
780 regeneration rates (Blomqvist et al., 1994; Hampel et al., 2019), and there can be an inverse
781 relationship between ammonium and MC concentrations (Kelly et al., 2019).
782 The MC:chl *a* and MC:cyanobacteria-chl *a* gave similar results for the 7 August 2019
783 HABs Grab because cyanobacteria dominated the phytoplankton community and green algae and
784 diatoms were in low concentration. On the 9 August 2018 HABs Grab, MC:Chl *a* ranged up to
785 0.3, whereas MC:cyanobacteria-chl *a* was between 0.1 and 0.6. Green algae and diatoms were in
786 relatively greater concentrations during the 2018 HABs Grab, and their contribution to total chl *a*
787 decreased MC:Chl *a*. MC:cyanobacteria-chl *a* on 9 August 2018 was on average about double
788 that of 7 August 2019 HABs Grab, which suggests the cyanobacteria on 9 August 2018 were
789 more toxic than on 7 August 2019. However, year-to-year comparisons are difficult with one-day
790 snapshots. Bloom progression, nitrogen availability, light climate histories, and water
791 temperature (Gobler et al., 2016; Kardinaal et al., 2007; Kitchens et al., 2018; Martin et al.,
792 2020) would have interacted to result in the MC to chl *a* ratio observed on the HABs Grab, and
793 we would have observed different ratios if the HABs Grab were conducted earlier or later in the
794 bloom.
795
796 *4.4. CyanoHAB metric comparison*
797 Finding that many cyanoHAB biomass metrics correlated was not surprising and should
798 have raised alarms if they did not correlate. However, correlation coefficients differed between
799 the two years, which is problematic for comparing data across multiple metrics and years. The
800 two parameters that had the lowest correlations with other parameters were chl RFU from the
801 handheld sonde and PC concentration extracted from filters. It is also important to note the chl

RFU did not correlate with chl *a* concentrations and PC RFU did not correlate with PC concentrations, and previous studies have highlighted the lack of correlation between handheld sensors and traditional methods (Cotterill et al., 2019; Hodges et al., 2017). While handheld fluorometers and filter extractions quantify the same pigments, fundamental differences will affect the data. The physiological state of the cells will impact the amount of fluorescence per cell, increasing it under stressful conditions such as low nutrients and photo-inhibition (Campbell et al., 1998). The morphology of the cyanobacterial colonies (single cell, small colonies, large colonies) affects the fluorescence signals, especially when large colonies drift in front of the sensor (Hodges et al., 2017). Finally, the amount of PC and chl *a* per cell is variable, with PC being much more variable than chl *a*, and is affected by light climate history (Chaffin et al., 2012), nutrient status (Beardall et al., 2001; Kirk, 1994), and growth phase (Chang et al., 2012). That variability likely explains the result that chl *a* has stronger relationships with MC, 16S rRNA, and *mcyE* concentrations than does PC. Given how PC and chl *a* fluorescence signals and cellular content are affected by environmental parameters, care must be taken when comparing dataset with different pigment-based metrics.

Both ADDA-ELISA and targeted LC-MS/MS have been used to quantify concentration of MCs in natural waters with each platform having its own sets of strengths and weaknesses. The ADDA-hapten is a conserved amino acid in MCs and is responsible for the primary mode of toxicity by inhibiting protein phosphatase 1 and 2a. To make an ELISA have cross-reactivity with all MCs, the ADDA-hapten was used to create an ADDA antibody (Fischer et al., 2001). The disadvantage with the ADDA-ELISA is that the cross-reactivity with several prevalent MCs produces artificially high concentrations (Guo et al., 2017; Thees et al., 2019). The target LC-MS/MS platform provides the concentrations for twelve MCs with standards. The primary

825 weakness is that there are hundreds of MC congeners (Spoof and Catherine, 2017), and the
826 potential of not quantifying all the prevalent MCs is real. As in this study, several other studies
827 report ADDA-ELISA to have a higher total MC concentration than the LC-MS/MS platform
828 (Birbeck et al., 2019; Foss and Aubel, 2015; Guo et al., 2017; Thees et al., 2019). Three
829 explanations for this scenario are: 1) the standards are not available for MCs in the bloom and
830 not quantitated by LC-MS/MS (Foss and Aubel, 2015), 2) degradation products such as ADDA
831 tetrapeptide, ADDA, and linear chain are present and cross-react with ADDA-ELISA (Thees et
832 al., 2019), and 3) several of the prevalent MCs with standards have cross-reactivities are higher
833 than 100% (Fischer et al., 2001; Guo et al., 2017). The MC congeners detected during the HABs
834 Grabs (Supplemental Fig. 4) agree with recent 2016-2017 Lake Erie MC congener studies, in
835 which the four major MC congeners were MC-RR, MC-LR, MC-YR and MC-LA (Matson et al.,
836 2020; Palagama et al., 2020). Over 21 MCs were present in 2016 and 2017 blooms (Palagama et
837 al., 2020) and unknown MC congeners were reported in the 2015 bloom (Foss and Aubel, 2015),
838 thus these data support that the ADDA-ELISA is detecting MC congeners that do not have
839 commercially available standards. Since the MC congeners have a wide range of toxicity and
840 have differing fate and transport because of the wide range of hydrophobicity, it is important to
841 identify the prevalent MCs in Lake Erie and make standards available.
842
843 *4.5. Lessons learned from the HABs Grab*
844 The HABs Grab highlighted limitations of the current cyanoHABs monitoring network,
845 but the collection and laboratory processing of 100 (or 172) water samples in one day is not
846 feasible to conduct on a routine basis. The majority of water samples collected in Lake Erie for
847 long-term monitoring of water quality are from fixed locations that are sampled at a variable

frequency ranging from weekly to seasonally. While this type of sampling scheme produces useful temporal data, it lacks spatial resolution and could miss essential areas of the bloom, like the 'finger' of biomass and MCs extending into Canadian waters observed in 2019 (Fig. 2). There are several potential options to overcome the spatial resolution limitation. Obviously, remote sensing can be used as a proxy for cyanobacterial biomass data over large spatial areas, but it cannot measure MCs directly (Stumpf et al., 2016a) and the spatial heterogeneity of MC:Chl *a* documented here suggests there would be significant uncertainty introduced when using a fixed ratio to extrapolate MCs from Chl *a* distributions. Gliders and autonomous underwater vehicles (AUV), such as the third generation of the environmental sample processor (ESP), can collect data and samples in areas of the lake not routinely sampled and transmit the data wirelessly to researchers and managers (Anderson et al., 2019; Scholin et al., 2017). Volunteers and citizen scientists can be trained to collect and process samples. For example, NOAA's phytoplankton monitoring network and OSU Stone Lab's charter boat water sampling program are citizen science projects; however, these volunteers need their own boats to collect offshore samples. Finally, the advancement of drones may facilitate the collection of water samples from bloom hot spots or areas not monitored by scientists, but drone technology is still in its infancy (Lally et al., 2019). While these options to overcome limitations of spatial resolution can augment routine monitoring programs and remote sensing, they do not replace existing methods. Therefore, it is paramount to develop and validate models that can forecast MCs over a large spatial area.

Our HABs Grab events occurred in an aquatic environment with the primary goal of quantifying the total mass of MCs, but the methods we used can be applied to other environments. Future efforts could expand this event to encompass connecting channels

impacted by cyanobacterial blooms, including the Maumee River and the Detroit River-Lake St. Clair-Thames River continuum (Davis et al., 2014; Matson et al., 2020; McKay et al., 2020), priority systems for the United States and Canadian governments, respectively. Environment and Climate Change Canada's already strong presence in the latter could be leveraged in these future efforts and benefit from the models suggested above. Likewise, HABs Grab-like methods can be used in the watershed to identify hot spots of nutrient loss from fields and other high contributors of nutrients.

Coordination of the HABs Grab in 2019 presented a few challenges. For the HABs Grab to occur on a particular date, we needed: 1) crewed vessels, 2) sufficient lab personnel and equipment to process all samples the day of collection, 3) favorable weather for the smaller vessels to safely and quickly transit their assigned sectors, and 4) a cyanoHAB present in the lake. Added value to the HABs Grab dataset was presented by 5) cloud-free conditions to validate satellite-derived bloom products. Early during planning, we targeted the first two weeks of August for the HABs Grab because there are cyanobacteria present in the western basin, albeit with much interannual variation in biomass in early August (Bridgeman et al., 2013), and university researchers are available prior to the return to classes in late-August. Then we surveyed interested groups for their availability during the first two weeks of August and picked several dates to conduct the HABs Grab when most groups were available. We also came to an understanding that not all groups might be available on the date selected. On the first Monday of our two-week window, we met at the Lake Erie Center for a logistics meeting, distributed sample equipment, and set up sample filtering stations to facilitate efficient sample processing. We monitored weather forecasts and sampled on the first decent weather day even though all groups might not have been available. We took this approach because we did not want to risk passing up

894 the opportunity to collect 175 samples on a decent day for potentially collecting 200 samples, for
895 example, on a later date that could get canceled due to storms. The decision to sample was made
896 on the day prior to the event. The short notice decision was challenging for the researchers
897 involved and even extended to the media wishing to cover the binational event. Overall, future
898 HABs Grab-like events can be successful if logistics are thoroughly planned, and there is an
899 understanding that not all involved may be able to participate, given the constraints of the
900 particular project. These exercises also represent a valuable way to involve media on both sides
901 of the border, thereby increasing public awareness and understanding of cyanoHAB and MC
902 issues in Lake Erie and reducing the likelihood of an 'out-of-sight, out-of-mind' mentality
903 among members of the public.
904
905 *4.5 Conclusions*
906 There was an estimated 11,513 kg and 30,691 kg of MCs in the western basin of Lake
907 Erie on a single day during peak cyanoHAB conditions on 9 August 2018 and 7 August 2019,
908 respectively. These estimates were made possible with a high spatial resolution dataset collected
909 throughout the entire basin using consistent methods. The fact that cyanoHABs can produce tons
910 of toxins can be alarming; therefore, these numbers must be put into context when messaging to
911 managers and the public. For example, the high MC mass estimates are a function of bloom
912 expanse and the large area of the basin (~2780 km^2) that is prone to cyanoHABs. The basin-wide
913 average estimated concentration was 0.52 µg/L and 1.38 µg/L, respectively, if the bloom was
914 spread throughout the basin. The bloom boundary poses substantial issues for spatial
915 interpolations because MC concentration can vary by nearly two orders of magnitude over very
916 short distances. The dataset also showed that the MC:chl *a* ratio varied by a factor up to 5.3

917 throughout the basin, creating challenges for using the ratio to predict MC concentrations. These
918 issues can only be overcome with more frequent data collection. Models designed to forecast
919 MC concentrations must account for the spatial heterogeneity in MC:chl *a* and the rapid
920 gradients at the bloom boundary. Furthermore, the HABs Grabs dataset will continue to be
921 utilized in upcoming studies ranging from molecular characterization of the microbial
922 communities, more detailed toxin analysis, ecosystem modeling, water mass and cyanoHAB
923 transport, and remote sensing validation.
924

925 **Acknowledgements**

926 This research was funded by the National Oceanic and Atmospheric Administration's National
927 Centers for Coastal Ocean Science under award NA17NOS4780186 to the Ohio State
928 University. This work was partially supported by funding from the National Institutes of Health
929 (NIH) (1P01ES028939-01) and National Science Foundation (OCE-1840715) awards to the
930 Bowling Green State University Great Lakes Center for Fresh Waters and Human Health, NIH to
931 Wayne State University for the Center for Urban Responses to Environmental Stressors (P30
932 ES020957), Natural Sciences and Engineering Research Council of Canada Discovery grants to
933 Canadian faculty, Great Lakes Program funding from Fisheries and Oceans for the operation of
934 the R.V. Cisco and Captain Robert D. Linley. This work was in part supported by the U.S.
935 Environmental Protection Agency (EPA) and any opinions expressed do not reflect the views of
936 the agency; therefore, no official endorsement should be inferred. Any mention of trade names or
937 commercial products does not constitute endorsement or recommendation for use. We greatly
938 appreciate the NOAA Great Lake Environmental Research Laboratory and the Cooperative
939 Institute for Great Lakes Research for vessel use and support of our project. We thank the boat

captains and dozens of students and laboratory technicians who helped during sample collection and sample processing on the dates of the HABs Grabs. This is contribution ##### from NOAA NCCOS awards.

References

Al-Tebrineh, J., Pearson, L.A., Yasar, S.A., Neilan, B.A., 2012. A multiplex qPCR targeting hepato- and neurotoxigenic cyanobacteria of global significance. Harmful Algae 15, 19–25. https://doi.org/10.1016/j.hal.2011.11.001

Anderson, C.R., Berdalet, E., Kudela, R.M., Cusack, C.K., Silke, J., O'Rourke, E., Dugan, D., McCammon, M., Newton, J.A., Moore, S.K., Paige, K., Ruberg, S., Morrison, J.R., Kirkpatrick, B., Hubbard, K., Morell, J., 2019. Scaling up from regional case studies to a global harmful algal bloom observing system. Front. Mar. Sci. 6. https://doi.org/10.3389/fmars.2019.00250

Anderson, E.J., Bechle, A.J., Wu, C.H., Schwab, D.J., Mann, G.E., Lombardy, K.A., 2015. Reconstruction of a meteotsunami in Lake Erie on 27 May 2012: Roles of atmospheric conditions on hydrodynamic response in enclosed basins. J. Geophys. Res. Oceans 120, 8020–8038. https://doi.org/10.1002/2015JC010883

Beardall, J., Young, E., Roberts, S., 2001. Approaches for determining phytoplankton nutrient limitation. Aquat. Sci. 63, 44–69.

Beutler, M., Wiltshire, K.H., Meyer, B., Moldaenke, C., Lüring, C., Meyerhöfer, M., Hansen, U.P., Dau, H., 2002. A fluorometric method for the differentiation of algal populations in vivo and in situ. Photosynth. Res. 72, 39–53.

Binding, C.E., Pizzolato, L., Zeng, C., 2021. EOLakeWatch; delivering a comprehensive suite of remote sensing algal bloom indices for enhanced monitoring of Canadian eutrophic lakes. Ecol. Indic. 121, 106999. https://doi.org/10.1016/j.ecolind.2020.106999

Birbeck, J.A., Westrick, J.A., O'Neill, G.M., Spies, B., Szlag, D.C., 2019. Comparative analysis of microcystin prevalence in Michigan Lakes by online concentration LC/MS/MS and ELISA. Toxins 11, 13. https://doi.org/10.3390/toxins11010013

Blomqvist, P., Petterson, A., Hyenstrand, P., 1994. Ammonium-nitrogen: A key regulatory factor causing dominance of non-nitrogen-fixing cyanobacteria in aquatic systems. Arch. Für Hydrobiol. 132, 141–164.

Brandenburg, K., Siebers, L., Keuskamp, J., Jephcott, T.G., Van de Waal, D.B., 2020. Effects of nutrient limitation on the synthesis of N-rich phytoplankton toxins: A Meta-Analysis. Toxins 12, 221. https://doi.org/10.3390/toxins12040221

976 Bridgeman, T.B., Chaffin, J.D., Filbrun, J.E., 2013. A novel method for tracking western Lake
977 Erie *Microcystis* blooms, 2002–2011. J. Gt. Lakes Res. 39, 83–89.

978 Bridgeman, T.B., Chaffin, J.D., Kane, D.D., Conroy, J.D., Panek, S.E., Armenio, P.M., 2012.
979 From River to Lake: Phosphorus partitioning and algal community compositional
980 changes in Western Lake Erie. J. Gt. Lakes Res. 38, 90–97.

981

982 Campbell, D., Hurry, V., Clarke, A.K., Gustafsson, P., Oquist, G., 1998. Chlorophyll
983 fluorescence analysis of cyanobacterial photosynthesis and acclimation. Microbiol. Mol.
984 Biol. Rev. 62, 667–683.

985 Carmichael, W. w., 1992. Cyanobacteria secondary metabolites—the cyanotoxins. J. Appl.
986 Bacteriol. 72, 445–459. https://doi.org/10.1111/j.1365-2672.1992.tb01858.x

987 Carmichael, W.W., Boyer, G.L., 2016. Health impacts from cyanobacteria harmful algae
988 blooms: Implications for the North American Great Lakes. Harmful Algae, global
989 expansion of harmful cyanobacterial blooms: Diversity, ecology, causes, and controls 54,
990 194–212. https://doi.org/10.1016/j.hal.2016.02.002

991 Chaffin, J.D., Bridgeman, T.B., Bade, D.L., 2013. Nitrogen constrains the growth of late summer
992 cyanobacterial blooms in Lake Erie. Adv. Microbiol. 03, 16–26.
993 https://doi.org/10.4236/aim.2013.36A003

994 Chaffin, J.D., Bridgeman, T.B., Heckathorn, S.A., Krause, A.E., others, 2012. Role of suspended
995 sediments and mixing in reducing photoinhibition in the bloom-forming cyanobacterium
996 *Microcystis*. J. Water Resour. Prot. 4, 1029.

997 Chaffin, J.D., Davis, T.W., Smith, D.J., Baer, M.M., Dick, G.J., 2018a. Interactions between
998 nitrogen form, loading rate, and light intensity on *Microcystis* and *Planktothrix* growth
999 and microcystin production. Harmful Algae 73, 84–97.
1000 https://doi.org/10.1016/j.hal.2018.02.001

1001 Chaffin, J.D., Kane, D.D., Stanislawczyk, K., Parker, E.M., 2018b. Accuracy of data buoys for
1002 measurement of cyanobacteria, chlorophyll, and turbidity in a large lake (Lake Erie,
1003 North America): implications for estimation of cyanobacterial bloom parameters from
1004 water quality sonde measurements. Environ. Sci. Pollut. Res. 25, 25175–25189.
1005 https://doi.org/10.1007/s11356-018-2612-z

1006 Chang, D.-W., Hobson, P., Burch, M., Lin, T.-F., 2012. Measurement of cyanobacteria using in-
1007 vivo fluoroscopy – Effect of cyanobacterial species, pigments, and colonies. Water Res.
1008 46, 5037–5048. https://doi.org/10.1016/j.watres.2012.06.050

1009 Chen, C., Liu, H., Beardsley, R.C., 2003. An unstructured grid, finite-volume, three-dimensional,
1010 primitive equations ocean model: application to coastal ocean and estuaries. J.
1011 Atmospheric Ocean. Technol. 20, 159–186. https://doi.org/10.1175/1520-
1012 0426(2003)020<0159:AUGFVT>2.0.CO;2

1013 Cotterill, V., Hamilton, D.P., Puddick, J., Suren, A., Wood, S.A., 2019. Phycocyanin sensors as
1014 an early warning system for cyanobacteria blooms concentrations: a case study in the
1015 Rotorua lakes. N. Z. J. Mar. Freshw. Res. 53, 555–570.
1016 https://doi.org/10.1080/00288330.2019.1617322

1017 Davis, T.W., Harke, M.J., Marcoval, Ma., Goleski, J., Orano-Dawson, C., Berry, D.L., Gobler,
1018 C.J., others, 2010. Effects of nitrogenous compounds and phosphorus on the growth of
1019 toxic and non-toxic strains of *Microcystis* during cyanobacterial blooms. Aquat. Microb.
1020 Ecol. 61, 149.

1021 Davis, T.W., Stumpf, R., Bullerjahn, G.S., McKay, R.M.L., Chaffin, J.D., Bridgeman, T.B.,
1022 Winslow, C., 2019. Science meets policy: A framework for determining impairment
1023 designation criteria for large waterbodies affected by cyanobacterial harmful algal
1024 blooms. Harmful Algae 81, 59–64. https://doi.org/10.1016/j.hal.2018.11.016

1025 Davis, T.W., Watson, S.B., Rozmarynowycz, M.J., Ciborowski, J.J., McKay, R.M., Bullerjahn,
1026 G.S., 2014. Phylogenies of microcystin-producing cyanobacteria in the lower Laurentian
1027 Great Lakes suggest extensive genetic connectivity. PloS One 9, e106093.

1028 Fang, S., Del Giudice, D., Scavia, D., Binding, C.E., Bridgeman, T.B., Chaffin, J.D., Evans,
1029 M.A., Guinness, J., Johengen, T.H., Obenour, D.R., 2019. A space-time geostatistical
1030 model for probabilistic estimation of harmful algal bloom biomass and areal extent. Sci.
1031 Total Environ. 695, 133776. https://doi.org/10.1016/j.scitotenv.2019.133776

1032 Fischer, W.J., Garthwaite, I., Miles, C.O., Ross, K.M., Aggen, J.B., Chamberlin, A.R., Towers,
1033 N.R., Dietrich, D.R., 2001. Congener-independent immunoassay for microcystins and
1034 nodularins. Environ. Sci. Technol. 35, 4849–4856. https://doi.org/10.1021/es011182f

1035 Foss, A.J., Aubel, M.T., 2015. Using the MMPB technique to confirm microcystin
1036 concentrations in water measured by ELISA and HPLC (UV, MS, MS/MS). Toxicon
1037 104, 91–101.

1038 GLWQA, 2015. Recommended phosphorus loading targets for Lake Erie - Annex 4 Objectives
1039 and Targets Task Team Final Report to the Nutrients Annex Subcommittee.

1040 Gobler, C.J., Burkholder, J.M., Davis, T.W., Harke, M.J., Johengen, T., Stow, C.A., Van de
1041 Waal, D.B., 2016. The dual role of nitrogen supply in controlling the growth and toxicity
1042 of cyanobacterial blooms. Harmful Algae, global expansion of harmful cyanobacterial
1043 blooms: Diversity, ecology, causes, and controls 54, 87–97.
1044 https://doi.org/10.1016/j.hal.2016.01.010

1045 Golnick, P.C., Chaffin, J.D., Bridgeman, T.B., Zellner, B.C., Simons, V.E., 2016. A comparison
1046 of water sampling and analytical methods in western Lake Erie. J. Gt. Lakes Res. 42,
1047 965–971. https://doi.org/10.1016/j.jglr.2016.07.031

1048 Graham, J.L., Dubrovsky, N.M., Foster, G.M., King, L.R., Loftin, K.A., Rosen, B.H., Stelzer,
1049 E.A., 2020. Cyanotoxin occurrence in large rivers of the United States. Inland Waters 10,
1050 109–117. https://doi.org/10.1080/20442041.2019.1700749

1051 Guo, Y.C., Lee, A.K., Yates, R.S., Liang, S., Rochelle, P.A., 2017. Analysis of microcystins in
1052 drinking water by ELISA and LC/MS/MS. J. AWWA 109, 13–25.
1053 https://doi.org/10.5942/jawwa.2017.109.0027

1054 Hampel, J.J., McCarthy, M.J., Neudeck, M., Bullerjahn, G.S., McKay, R.M.L., Newell, S.E.,
1055 2019. Ammonium recycling supports toxic *Planktothrix* blooms in Sandusky Bay, Lake
1056 Erie: Evidence from stable isotope and metatranscriptome data. Harmful Algae 81, 42–
1057 52. https://doi.org/10.1016/j.hal.2018.11.011

Harke, M.J., Steffen, M.M., Gobler, C.J., Otten, T.G., Wilhelm, S.W., Wood, S.A., Paerl, H.W., 2016. A review of the global ecology, genomics, and biogeography of the toxic cyanobacterium, *Microcystis* spp. Harmful Algae, global expansion of harmful cyanobacterial blooms: Diversity, ecology, causes, and controls 54, 4–20. https://doi.org/10.1016/j.hal.2015.12.007

He, X., Liu, Y.-L., Conklin, A., Westrick, J., Weavers, L.K., Dionysiou, D.D., Lenhart, J.J., Mouser, P.J., Szlag, D., Walker, H.W., 2016. Toxic cyanobacteria and drinking water: Impacts, detection, and treatment. Harmful Algae, global expansion of harmful cyanobacterial blooms: Diversity, ecology, causes, and controls 54, 174–193. https://doi.org/10.1016/j.hal.2016.01.001

Herdendorf, C.E., 1982. Large Lakes of the World. J. Gt. Lakes Res. 8, 379–412. https://doi.org/10.1016/S0380-1330(82)71982-3

Hodges, C.M., Wood, S.A., Puddick, J., McBride, C.G., Hamilton, D.P., 2017. Sensor manufacturer, temperature, and cyanobacteria morphology affect phycocyanin fluorescence measurements. Environ. Sci. Pollut. Res. 1–10. https://doi.org/10.1007/s11356-017-0473-5

Horst, G.P., Sarnelle, O., White, J.D., Hamilton, S.K., Kaul, R.B., Bressie, J.D., 2014. Nitrogen availability increases the toxin quota of a harmful cyanobacterium, *Microcystis aeruginosa*. Water Res. 54, 188–198.

Kardinaal, W.E.A., Tonk, L., Janse, I., Hol, S., Slot, P., Huisman, J., Visser, P.M., 2007. Competition for light between toxic and nontoxic strains of the harmful cyanobacterium *Microcystis*. Appl. Environ. Microbiol. 73, 2939–2946. https://doi.org/10.1128/AEM.02892-06

Kelly, N.E., Javed, A., Shimoda, Y., Zastepa, A., Watson, S., Mugalingam, S., Arhonditsis, G.B., 2019. A Bayesian risk assessment framework for microcystin violations of drinking water and recreational standards in the Bay of Quinte, Lake Ontario, Canada. Water Res. 162, 288–301. https://doi.org/10.1016/j.watres.2019.06.005

Kirk, J.T.O., 1994. Light and photosynthesis in aquatic ecosystems, 2nd, illustrated, revised ed. Cambridge University Press, Cambridge [England] ; New York, NY, USA.

Kitchens, C.M., Johengen, T.H., Davis, T.W., 2018. Establishing spatial and temporal patterns in Microcystis sediment seed stock viability and their relationship to subsequent bloom development in Western Lake Erie. PLOS ONE 13, e0206821. https://doi.org/10.1371/journal.pone.0206821

Kramer, E.L., 2018. Diel Vertical distribution of *Microcystis* and associated environmental factors in the western basin of Lake Erie. University of Toledo.

Krausfeldt, L.E., Steffen, M.M., McKay, R.M., Bullerjahn, G.S., Boyer, G.L., Wilhelm, S.W., 2019. Insight into the molecular mechanisms for microcystin biodegradation in Lake Erie and Lake Taihu. Front. Microbiol. 10. https://doi.org/10.3389/fmicb.2019.02741

Kutovaya, O.A., McKay, R.M.L., Beall, B.F., Wilhelm, S.W., Kane, D.D., Chaffin, J.D., Bridgeman, T.B., Bullerjahn, G.S., 2012. Evidence against fluvial seeding of recurrent toxic blooms of *Microcystis* spp. in Lake Erie's western basin. Harmful Algae 15, 71–77.

1099 Lally, H.T., O'Connor, I., Jensen, O.P., Graham, C.T., 2019. Can drones be used to conduct
1100 water sampling in aquatic environments? A review. Sci. Total Environ. 670, 569–575.
1101 https://doi.org/10.1016/j.scitotenv.2019.03.252

1102 Liu, Q., Rowe, M.D., Anderson, E.J., Stow, C.A., Stumpf, R.P., Johengen, T.H., 2020.
1103 Probabilistic forecast of microcystin toxin using satellite remote sensing, in situ
1104 observations and numerical modeling. Environ. Model. Softw. 128, 104705.
1105 https://doi.org/10.1016/j.envsoft.2020.104705

1106 Loftin, K.A., Graham, J.L., Hilborn, E.D., Lehmann, S.C., Meyer, M.T., Dietze, J.E., Griffith,
1107 C.B., 2016. Cyanotoxins in inland lakes of the United States: Occurrence and potential
1108 recreational health risks in the EPA National Lakes Assessment 2007. Harmful Algae 56,
1109 77–90. https://doi.org/10.1016/j.hal.2016.04.001

1110 Martin, R.M., Moniruzzaman, M., Stark, G.F., Gann, E.R., Derminio, D.S., Wei, B., Hellweger,
1111 F.L., Pinto, A., Boyer, G.L., Wilhelm, S.W., 2020. Episodic decrease in temperature
1112 increases *mcy* gene transcription and cellular microcystin in continuous cultures of
1113 *Microcystis aeruginosa* PCC 7806. Front. Microbiol. 11.
1114 https://doi.org/10.3389/fmicb.2020.601864

1115 Matson, P.G., Boyer, G.L., Bridgeman, T.B., Bullerjahn, G.S., Kane, D.D., McKay, R.M.L.,
1116 McKindles, K.M., Raymond, H.A., Snyder, B.K., Stumpf, R.P., Davis, T.W., 2020.
1117 Physical drivers facilitating a toxigenic cyanobacterial bloom in a major Great Lakes
1118 tributary. Limnol. Oceanogr. n/a. https://doi.org/10.1002/lno.11558

1119 McKay, R.M., Frenken, T., Diep, N., Cody, W.R., Crevecoeur, S., Dove, A., Drouillard, K.G.,
1120 Ortiz, X., Wintermute, J., Zastepa, A., 2020. Bloom announcement: An early autumn
1121 cyanobacterial bloom co-dominated by *Aphanizomenon flos-aquae* and *Planktothrix*
1122 *agardhii* in an agriculturally-influenced Great Lakes tributary (Thames River, Ontario,
1123 Canada). Data Brief 30, 105585. https://doi.org/10.1016/j.dib.2020.105585

1124 McKindles, K., Frenken, T., McKay, R.M.L., Bullerjahn, G.S., 2020. Binational efforts
1125 addressing cyanobacterial harmful algal blooms in the Great Lakes. In: Crossman J.,
1126 Weisener C. (eds) Contaminants of the Great Lakes. The handbook of environmental
1127 chemistry, vol 101. Springer, Cham. https://doi.org/10.1007/698_2020_513

1128 Mellor, G.L., Yamada, T., 1982. Development of a turbulence closure model for geophysical
1129 fluid problems. Rev. Geophys. 20, 851–875. https://doi.org/10.1029/RG020i004p00851

1130 Michalak, A.M., Anderson, E.J., Beletsky, D., Boland, S., Bosch, N.S., Bridgeman, T.B.,
1131 Chaffin, J.D., Cho, K., Confesor, R., Daloğlu, I., DePinto, J.V., Evans, M.A., Fahnenstiel,
1132 G.L., He, L., Ho, J.C., Jenkins, L., Johengen, T.H., Kuo, K.C., LaPorte, E., Liu, X.,
1133 McWilliams, M.R., Moore, M.R., Posselt, D.J., Richards, R.P., Scavia, D., Steiner, A.L.,
1134 Verhamme, E., Wright, D.M., Zagorski, M.A., 2013. Record-setting algal bloom in Lake
1135 Erie caused by agricultural and meteorological trends consistent with expected future
1136 conditions. Proc. Natl. Acad. Sci. 110, 6448–6452.
1137 https://doi.org/10.1073/pnas.1216006110

1138 Millie, D.F., Fahnenstiel, G.L., Dyble Bressie, J., Pigg, R.J., Rediske, R.R., Klarer, D.M., Tester,
1139 P.A., Litaker, R.W., 2009. Late-summer phytoplankton in western Lake Erie (Laurentian
1140 Great Lakes): bloom distributions, toxicity, and environmental influences. Aquat. Ecol.
1141 43, 915–934.

1142 Ohio Environmental Protection Agency, 2018. Ohio EPA Total (Extracellular and Intracellular)
1143 Microcystins - ADDA by ELISA Analytical Methodology. Ohio EPA DES 701.0
1144 Version

1145 O'Neil, J.M., Davis, T.W., Burford, M.A., Gobler, C.J., 2012. The rise of harmful cyanobacteria
1146 blooms: The potential roles of eutrophication and climate change. Harmful Algae,
1147 Harmful Algae--The requirement for species-specific information 14, 313–334.
1148 https://doi.org/10.1016/j.hal.2011.10.027

1149 Paerl, H.W., Gardner, W.S., Havens, K.E., Joyner, A.R., McCarthy, M.J., Newell, S.E., Qin, B.,
1150 Scott, J.T., 2016. Mitigating cyanobacterial harmful algal blooms in aquatic ecosystems
1151 impacted by climate change and anthropogenic nutrients. Harmful Algae, global
1152 expansion of harmful cyanobacterial blooms: Diversity, ecology, causes, and controls 54,
1153 213–222. https://doi.org/10.1016/j.hal.2015.09.009

1154 Palagama, D.S.W., Baliu-Rodriguez, D., Snyder, B.K., Thornburg, J.A., Bridgeman, T.B.,
1155 Isailovic, D., 2020. Identification and quantification of microcystins in western Lake Erie
1156 during 2016 and 2017 harmful algal blooms. J. Gt. Lakes Res.
1157 https://doi.org/10.1016/j.jglr.2020.01.002

1158 Perz, S.G., Brilhante, S., Brown, I.F., Michaelsen, A.C., Mendoza, E., Passos, V., Pinedo, R.,
1159 Reyes, J.F., Rojas, D., Selaya, G., 2010. Crossing boundaries for environmental science
1160 and management: combining interdisciplinary, interorganizational and international
1161 collaboration. Environ. Conserv. 37, 419–431.
1162 https://doi.org/10.1017/S0376892910000810

1163 Philip, G.M., Watson, D.F., 1982. A precise methof for determining contoured surfaces. APPEA
1164 J. 22, 205–212. https://doi.org/10.1071/aj81016

1165 Qian, S.S., Chaffin, J.D., DuFour, M.R., Sherman, J.J., Golnick, P.C., Collier, C.D., Nummer,
1166 S.A., Margida, M.G., 2015. Quantifying and reducing uncertainty in estimated
1167 microcystin concentrations from the ELISA method. Environ. Sci. Technol. 49, 14221–
1168 14229. https://doi.org/10.1021/acs.est.5b03029

1169 Qin, B., Zhu, G., Gao, G., Zhang, Y., Li, W., Paerl, H.W., Carmichael, W.W., 2010. A drinking
1170 water crisis in Lake Taihu, China: linkage to climatic variability and lake management.
1171 Environ. Manage. 45, 105–112. https://doi.org/10.1007/s00267-009-9393-6

1172 Rinta-Kanto, J.M., Konopko, E.A., DeBruyn, J.M., Bourbonniere, R.A., Boyer, G.L., Wilhelm,
1173 S.W., 2009. Lake Erie *Microcystis*: Relationship between microcystin production,
1174 dynamics of genotypes and environmental parameters in a large lake. Harmful Algae,
1175 This issue contains the special section on "Strains" 8, 665–673.
1176 https://doi.org/10.1016/j.hal.2008.12.004

1177 Rowe, M.D., Anderson, E.J., Wynne, T.T., Stumpf, R.P., Fanslow, D.L., Kijanka, K.,
1178 Vanderploeg, H.A., Strickler, J.R., Davis, T.W., 2016. Vertical distribution of buoyant
1179 *Microcystis* blooms in a Lagrangian particle tracking model for short-term forecasts in
1180 Lake Erie. J. Geophys. Res. Oceans 121, 5296–5314.
1181 https://doi.org/10.1002/2016JC011720

1182 Sarada, R., Pillai, M.G., Ravishankar, G.A., 1999. Phycocyanin from *Spirulina* sp: influence of
1183 processing of biomass on phycocyanin yield, analysis of efficacy of extraction methods

and stability studies on phycocyanin. Process Biochem. 34, 795–801. https://doi.org/10.1016/S0032-9592(98)00153-8

Sayers, M., Fahnenstiel, G.L., Shuchman, R.A., Whitley, M., 2016. Cyanobacteria blooms in three eutrophic basins of the Great Lakes: a comparative analysis using satellite remote sensing. Int. J. Remote Sens. 37, 4148–4171. https://doi.org/10.1080/01431161.2016.1207265

Scholin, C.A., Birch, J., Jensen, S., Marin, R., Massion, E., Pargett, D., Preston, C., Roman, B., Ussler, W., 2017. The quest to develop ecogenomic sensors: A 25-year history of the environmental sample processor (ESP) as a case study. Oceanography 30, 100–113.

Schwab, D.J., Beletsky, D., DePinto, J., Dolan, D.M., 2009. A hydrodynamic approach to modeling phosphorus distribution in Lake Erie. J. Gt. Lakes Res. 35, 50–60.

Sitoki, L., Kurmayer, R., Rott, E., 2012. Spatial variation of phytoplankton composition, biovolume, and resulting microcystin concentrations in the Nyanza Gulf (Lake Victoria, Kenya). Hydrobiologia 691, 109–122. https://doi.org/10.1007/s10750-012-1062-8

Smagorinsky, J., 1963. General circulation experiments with the primitive equations. Mon. Weather Rev. 91, 99–164. https://doi.org/10.1175/1520-0493(1963)091<0099:GCEWTP>2.3.CO;2

Spoof, L., Catherine, A., 2017. Appendix 3: Tables of microcystins and nodularins, in: J. Meriluoto, L. Spoof, J. Codd (Eds.), Handbook of cyanobacterial monitoring and cyanotoxin analysis. Wiley, Hoboken, pp. 526–538.

Steffen, M.M., Belisle, B.S., Watson, S.B., Boyer, G.L., Wilhelm, S.W., 2014. Status, causes and controls of cyanobacterial blooms in Lake Erie. J Gt. Lakes Res 40, 215–225.

Steffen, M.M., Davis, T.W., McKay, R.M.L., Bullerjahn, G.S., Krausfeldt, L.E., Stough, J.M.A., Neitzey, M.L., Gilbert, N.E., Boyer, G.L., Johengen, T.H., Gossiaux, D.C., Burtner, A.M., Palladino, D., Rowe, M.D., Dick, G.J., Meyer, K.A., Levy, S., Boone, B.E., Stumpf, R.P., Wynne, T.T., Zimba, P.V., Gutierrez, D., Wilhelm, S.W., 2017. Ecophysiological examination of the Lake Erie *Microcystis* bloom in 2014: linkages between biology and the water supply shutdown of Toledo, OH. Environ. Sci. Technol. 51, 6745–6755. https://doi.org/10.1021/acs.est.7b00856

Stumpf, R.P., Davis, T.W., Wynne, T.T., Graham, J.L., Loftin, K.A., Johengen, T.H., Gossiaux, D., Palladino, D., Burtner, A., 2016a. Challenges for mapping cyanotoxin patterns from remote sensing of cyanobacteria. Harmful Algae, global expansion of harmful cyanobacterial blooms: Diversity, ecology, causes, and controls 54, 160–173. https://doi.org/10.1016/j.hal.2016.01.005

Stumpf, R.P., Johnson, L.T., Wynne, T.T., Baker, D.B., 2016b. Forecasting annual cyanobacterial bloom biomass to inform management decisions in Lake Erie. J. Gt. Lakes Res. 42, 1174–1183. https://doi.org/10.1016/j.jglr.2016.08.006

Stumpf, R.P., Wynne, T.T., Baker, D.B., Fahnenstiel, G.L., 2012. Interannual variability of cyanobacterial blooms in Lake Erie. PLoS One 7, e42444.

Thees, A., Atari, E., Birbeck, J., Westrick, J.A., Huntley, J.F., 2019. Isolation and characterization of Lake Erie bacteria that degrade the cyanobacterial microcystin toxin MC-LR. J. Gt. Lakes Res. 45, 138–149. https://doi.org/10.1016/j.jglr.2018.10.013

Thoisen, C., Hansen, B.W., Nielsen, S.L., 2017. A simple and fast method for extraction and quantification of cryptophyte phycoerythrin. MethodsX 4, 209–213. https://doi.org/10.1016/j.mex.2017.06.002

Van de Waal, D.B., Smith, V.H., Declerck, S.A.J., Stam, E.C.M., Elser, J.J., 2014. Stoichiometric regulation of phytoplankton toxins. Ecol. Lett. 17, 736–742. https://doi.org/10.1111/ele.12280

Verhamme, E.M., Redder, T.M., Schlea, D.A., Grush, J., Bratton, J.F., DePinto, J.V., 2016. Development of the western Lake Erie ecosystem model (WLEEM): Application to connect phosphorus loads to cyanobacteria biomass. J. Gt. Lakes Res. https://doi.org/10.1016/j.jglr.2016.09.006

Wagner, N.D., Osburn, F.S., Wang, J., Taylor, R.B., Boedecker, A.R., Chambliss, C.K., Brooks, B.W., Scott, J.T., 2019. Biological stoichiometry regulates toxin production in *Microcystis aeruginosa* (UTEX 2385). Toxins 11, 601.

Wang, H., Gruden, C.L., Bridgeman, T.B., Chaffin, J.D., 2009. Detection and quantification of *Microcystis* spp. and microcystin-LR in western Lake Erie during the summer of 2007. Water Sci. Technol. 60.

Watson, D.F., Philip, G.M., 1985. A refinement of inverse distance weighted interpolation. Geoprocessing 2, 315–327.

Wynne, T.T., Stumpf, R.P., 2015. Spatial and temporal patterns in the seasonal distribution of toxic cyanobacteria in western Lake Erie from 2002–2014. Toxins 7, 1649–1663.

Wynne, T.T., Stumpf, R.P., Tomlinson, M.C., Fahnenstiel, G.L., Dyble, J., Schwab, D.J., Joshi, S.J., 2013. Evolution of a cyanobacterial bloom forecast system in western Lake Erie: Development and initial evaluation. J. Gt. Lakes Res., Remote Sensing of the Great Lakes and Other Inland Waters 39, 90–99. https://doi.org/10.1016/j.jglr.2012.10.003

Xue, P., Pal, J.S., Ye, X., Lenters, J.D., Huang, C., Chu, P.Y., 2017. Improving the simulation of large lakes in regional climate modeling: Two-way lake–atmosphere coupling with a 3D hydrodynamic model of the Great Lakes. J. Clim. 30, 1605–1627. https://doi.org/10.1175/JCLI-D-16-0225.1

Table 1. Total microcystins mass (kg) in the western basin of Lake Erie during the two HABs Grabs events, the maximum and average (standard deviation in parenthesis) MC concentrations (μg/L) measured in water samples collected during the HABs Grab on 9 August 2018 and 7 August 2019, and theoretical basin-wide average concentration. The microcystin data were from the ELISA method.

			Average MC in samples		
	Total MCs (kg)	Max MC measured	All samples	In samples with detectable MC	Theoretical basin-wide
2018	11,513	6.38	1.81 (1.21)	1.94 (1.16)	0.52
2019	30,691	46.56	3.50 (6.77)	5.02 (7.70)	1.38

1281 Table 2. Pearson correlation coefficient (*r*) matrix among metrics used to estimate cyanobacterial biomass during the 9 August 2018
1282 and 7 August 2019 HABs Grab and the range of values observed. Strong (*r* = 0.71 to 0.90) and very strong (*r* > 0.90) correlations
1283 between two parameters are bolded. "NS" = not significant correlation (P > 0.05). ND = no data was recorded. *One 2018 outlier
1284 sample was removed from the correlation that had chl values approximately 2 to 3 times greater than the highest sample reported in
1285 the last column.

	Year	Chl RFU	PC RFU	Cyano. Chl *a*	Total chl *a*	Chl *a*	PC	16S	*mcyE*	Total MCs	Exc. MCs	Range of values*
Chlorophyll RFU - YSI	2018	1	**.85**	.51	**.75**	.54	ND	ND	NS	NS	-.21	0.30 – 3.67
	2019	1	.66	.65	.68	.70	.43	.66	.63	**.71**	.43	0.05 - 3.85
Phycocyanin RFU - YSI	2018	**.85**	1	.57	**.76**	.61	ND	ND	NS	NS	-.35	-0.06 – 2.90
	2019	.66	1	**.77**	**.78**	**.74**	.55	.62	.65	**.78**	.48	0.00 - 21.13
Cyanobacteria chlorophyll *a* µg/L - FluoroProbe	2018	.51	.57	1	**.86**	**.94**	ND	ND	NS	.73	NS	0.28 – 11.15
	2019	.65	**.77**	1	**.99**	**.98**	.54	**.92**	**.80**	**.90**	.60	0.43 - 110.40
Total chlorophyll *a* µg/L - FluoroProbe	2018	**.75**	**.76**	**.86**	1	**.90**	ND	ND	NS	.48	NS	2.82 – 20.99
	2019	.68	**.78**	**.99**	1	**.98**	.53	**.92**	**.79**	**.90**	.58	3.08 - 132.63
Chlorophyll *a* µg/L - filter extracted	2018	.54	.61	**.94**	**.90**	1	ND	ND	NS	.72	NS	3.50 – 31.76
	2019	.70	**.74**	**.98**	**.98**	1	.51	**.95**	**.83**	**.92**	.60	1.88 - 196.16
Phycocyanin µg/L - filter extracted	2018	ND	ND	ND	ND	ND	ND	ND	ND	ND	ND	No data
	2019	.43	.55	.54	.53	.51	1	.49	.55	.52	.42	0 - 18.22
Cyanobacteria 16S gene copies/L - qPCR	2018	ND	ND	ND	ND	ND	ND	ND	ND	ND	ND	No data
	2019	.66	.62	**.92**	**.92**	**.95**	.49	1	**.97**	**.89**	**.89**	$3.3*10^7$ - $7.5*10^8$
Cyanobacteria *mcyE* gene copies/L - qPCR	2018	NS	NS	NS	NS	NS	ND	ND	1	.40	.50	0 - $4.7*10^7$
	2019	.63	.65	**.80**	**.79**	**.83**	.55	**.97**	1	**.83**	.55	$3.1*10^4$ - $2.8*10^8$
Total Microcystins	2018	NS	NS	.73	.48	.72	ND	ND	.40	1	.24	<0.1 - 6.38

µg/L - ELISA	2019	**.71**	**.78**	**.90**	**.90**	**.92**	.52	**.89**	**.83**	1	.62	<0.1 - 46.56
Extracellular	2018	-.21	-.35	NS	NS	NS	ND	ND	.50	.24	1	<0.1 - 0.75
Microcystins µg/L-ELISA	2019	.43	.48	.60	.58	.60	.42	**.89**	.55	.62	1	<0.1 - 1.38

1286 Figure legends

1287

1288 Figure 1. Time series of cyanobacterial biomass and microcystins (A & B), 14 day rolling
1289 average bloom spatial extent (C & D), and total phytoplankton biomass and the relative
1290 abundance of green algae, cyanobacteria, diatoms, and cryptophytes (E & F) in western Lake
1291 Erie on 9 August 2018 and 7 August 2019. The values in A, B, E, and F are the mean of five
1292 sites (± 1 standard error) monitored by the University of Toledo's Lake Erie Center. The bold
1293 vertical line in each indicates the dates of the HABs Grab event and shows the event occurred
1294 during peak bloom conditions each year.

1295

1296 Figure 2. Cyanobacterial biomass and microcystins during the 9 August 2018 (left column) and 7
1297 August 2019 (right column) HABs Grab. Top row: NOAA Cyanobacterial Index taken on 5
1298 August 2018 and 7 August 2019. The heat map ranges from 20,000 cells/mL in dark blue to
1299 6,300,000 cells/mL in dark red. Black is cells not detected and gray is cloud cover. Second row:
1300 Chlorophyll *a* (µg/L, top). Third row: total microcystins measured by ELISA (µg/L, middle).
1301 Bottom row: the ratio of microcystins to chlorophyll *a*. Small dots on the maps represent the
1302 sample collection locations.

1303

1304 Figure 3. The percentage of the *Microcystis* population capable of producing microcystins
1305 (relative abundance of *mcy* genes counts normalized to the gene counts of the *Microcystis*-
1306 specific 16S derived from shotgun metagenome read-mapping) during the 9 August 2018 HABs
1307 Grab as a function of distance from the mouth of the Maumee River.

1308

Figure 4. The hydrodynamic conditions of the western basin during the 9 August 2018 (top) and 7 August 2019 HABs Grab as simulated with the Finite Volume Community Ocean Model (FVCOM).

Figure 5. Nutrient concentrations (µmol/L) measured during the HABs Grabs. Dissolved inorganic nitrogen (sum of nitrate, nitrite, and ammonium; top), total nitrogen (second row), total phosphorus (third row), and the ratio of total N to total P concentration (bottom) of the 9 August 2018 (left) and 7 August 2019 (right) HABs Grabs. Small dots on the maps represent the sample collection locations.

Figure 6. The relationship between total microcystins measured by ELISA and the calculated total microcystins from 13 different congeners during the 9 August 2018 (filled circles, solid regression line) and 7 August 2019 (open circles, dashed regression line) HABs Grab. The dotted line is a 1-to-1 line. The inset panel shows a zoomed in view of the lower range where most of the 2018 samples occurred. 2018 regression equation: LC-MS/MS = (0.5125 * ELISA) + 0.1596, $R^2 = 0.79$. 2019 regression equation: LC-MS/MS = (0.5462 * ELISA) + 0.3229, $R^2 = 0.95$.

Figure 7. Total microcystins (measured by ELISA) concentration (A) and the microcystins-to-chlorophyll ratio (B) as a function of chlorophyll *a* concentration for each year. 9 August 2018 regression equation: MC = (0.109 * Chl) + 0.955, $R^2 = 0.32$. 7 August 2019 regression equation: MC = (0.201 * Chl) – 0.927, $R^2 = 0.80$. During the large bloom year of 2019, higher chlorophyll *a* concentrations corresponded to high toxin-to-biomass ratios, but high toxin-to-biomass ratios were also observed at low chlorophyll *a* concentrations.

Figure 8. The relationships between microcystins (ELISA), chlorophyll *a,* the ratio of microcystins to chlorophyll *a* concentration, and residuals from the microcystins v. chlorophyll regression (Fig. 7A) with water temperature, pH, turbidity, and specific conductivity during the 9 August 2018 (black circles) and 7 August 2019 (white circles) HABs Grab for samples with greater than 1 µg/L of total microcystins.

Figure 9. The relationships between microcystins (ELISA), chlorophyll *a,* the ratio of microcystins to chlorophyll *a* concentration, and residuals from the microcystins v. chlorophyll regression (Fig. 7A) with total Kjeldhal nitrogen, dissolved inorganic nitrogen, total nitrogen, total phosphorus, and the total nitrogen-to-total phosphorus ratio during the 9 August 2018 (black circles) and 7 August 2019 (white circles) HABs Grab for samples with greater than 1 µg/L of total microcystins.

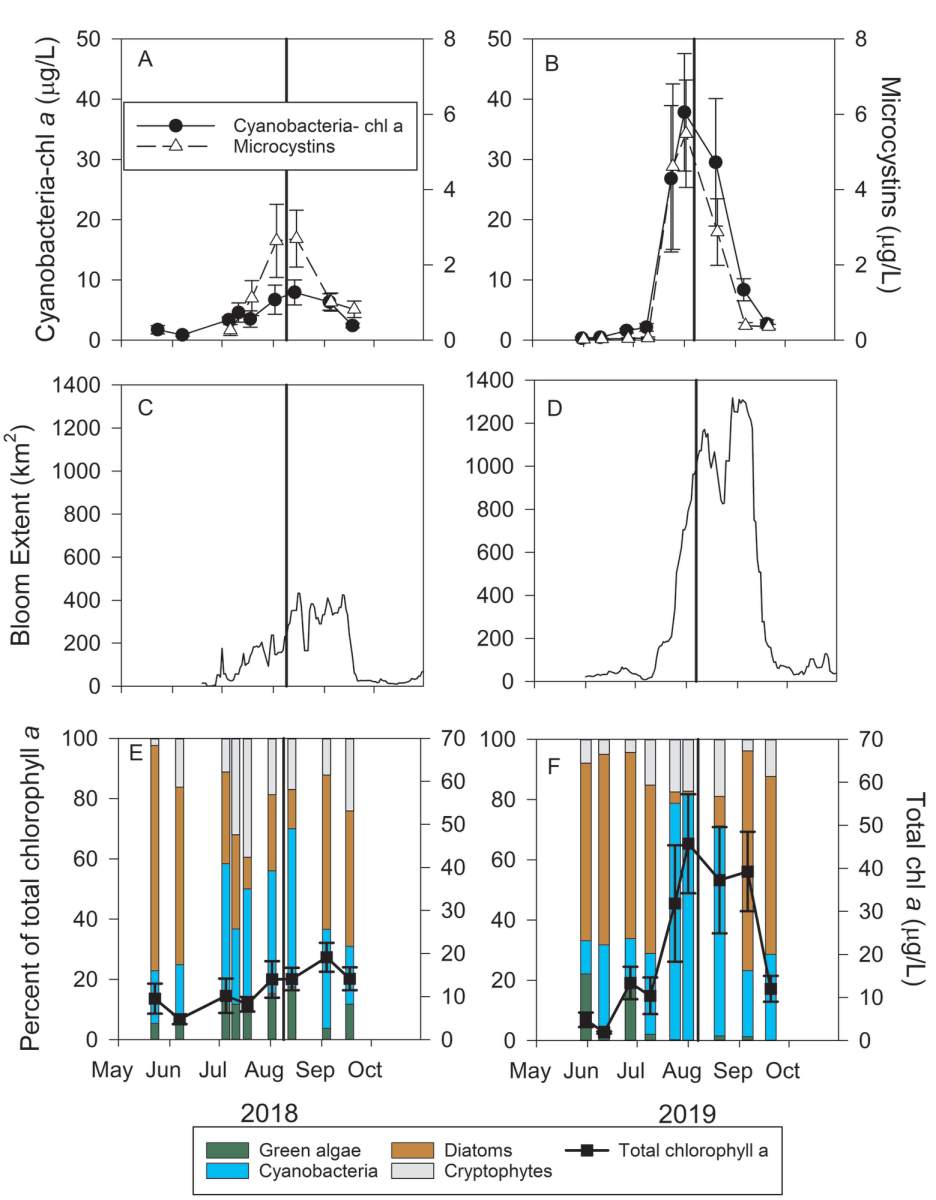
A
B
C
D
E
F
Cyanobacteria- chl a
Microcystins
Cyanobacteria-chl a (µg/L)
Microcystins (µg/L)
Bloom Extent (km2)
Percent of total chlorophyll a
Total chl a (µg/L)
May
Jun
Jul
Aug
Sep
Oct
2018
2019
Green algae
Cyanobacteria
Diatoms
Cryptophytes
Total chlorophyll a

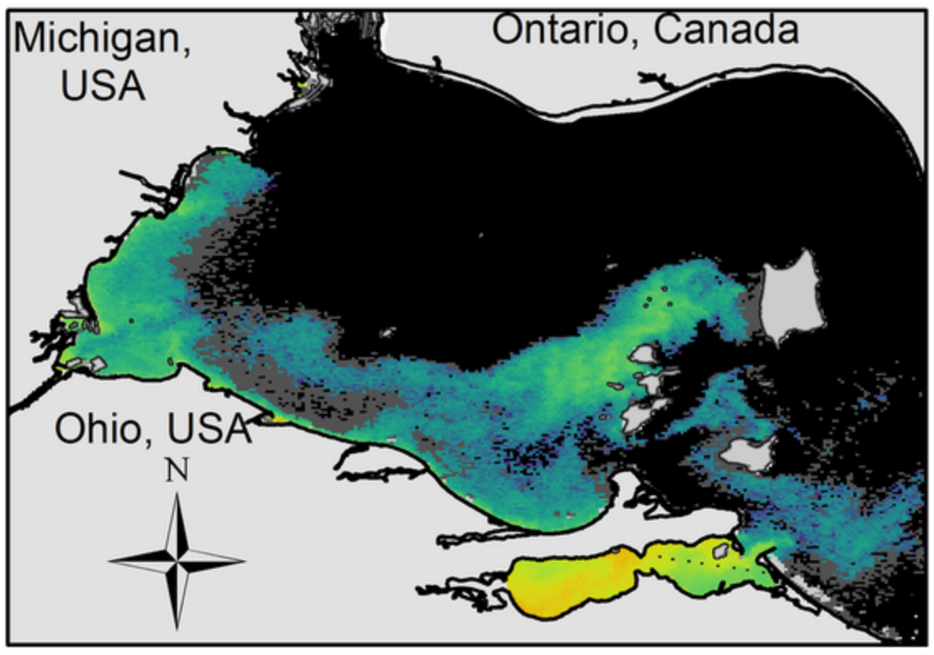
Michigan, USA
Ontario, Canada
Ohio, USA
N

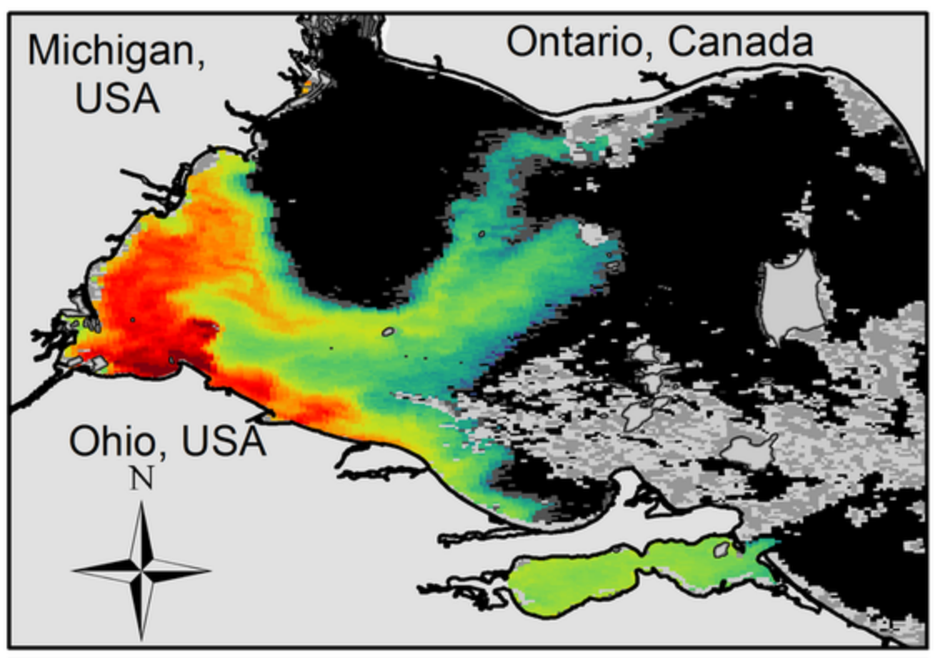
Michigan, USA
Ontario, Canada
Ohio, USA
N

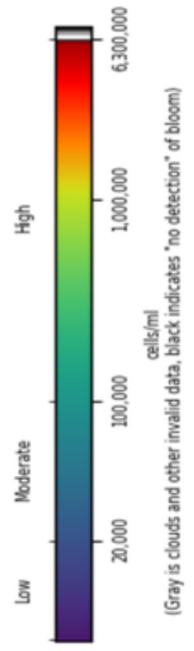
High
Moderate
Low
6,300,000
1,000,000
100,000
20,000
cells/ml
(Gray is clouds and other invalid data, black indicates "no detection" of bloom)

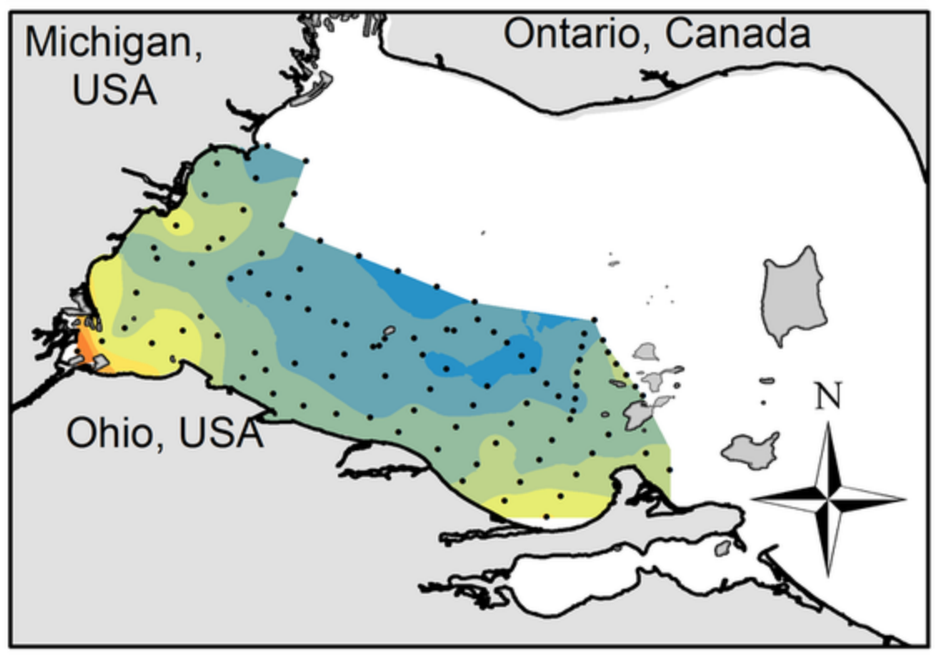
Michigan, USA
Ontario, Canada
Ohio, USA
N

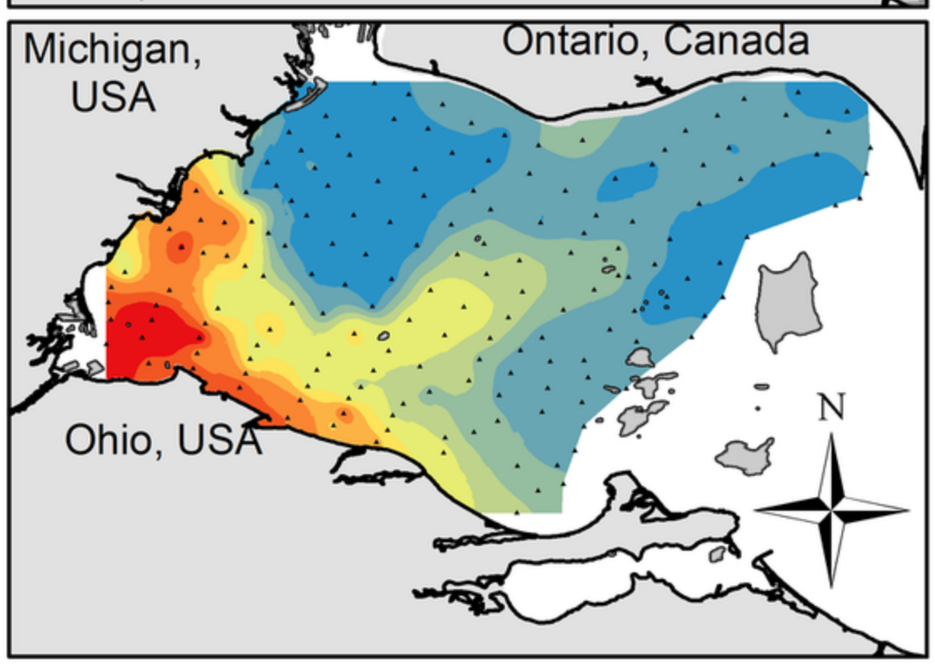
Michigan, USA
Ontario, Canada
Ohio, USA
N

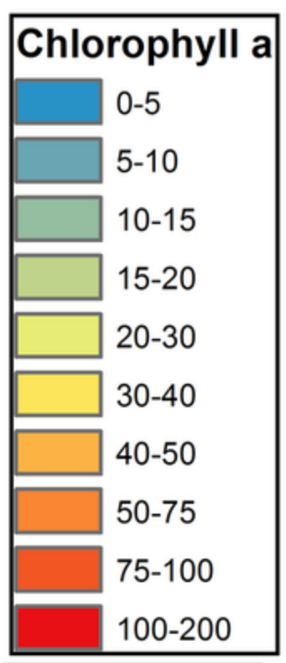
Chlorophyll a
0-5
5-10
10-15
15-20
20-30
30-40
40-50
50-75
75-100
100-200

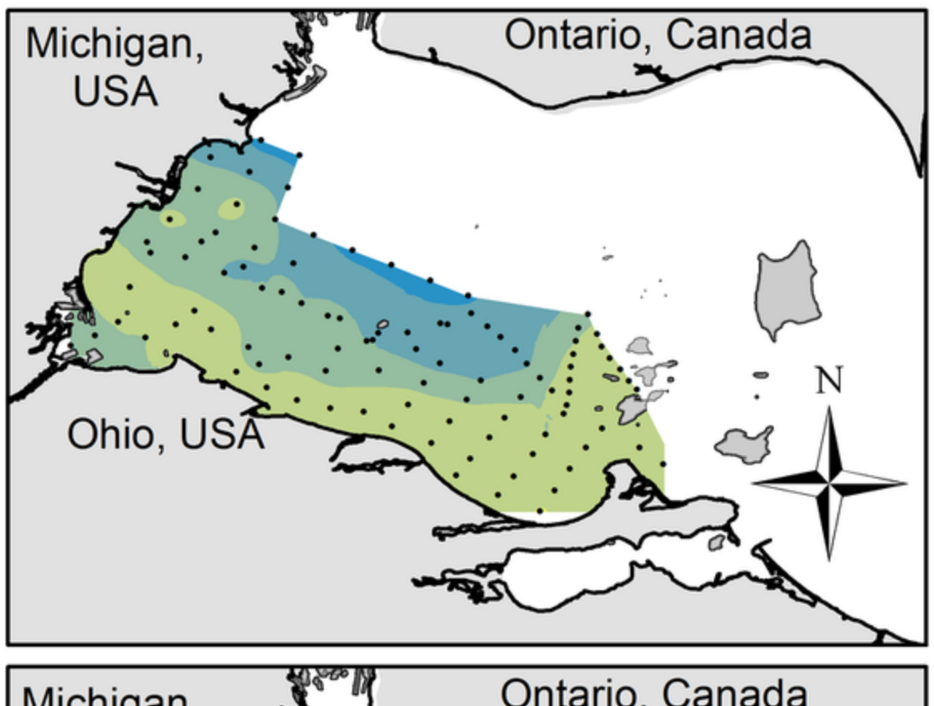
Michigan, USA
Ontario, Canada
Ohio, USA
N

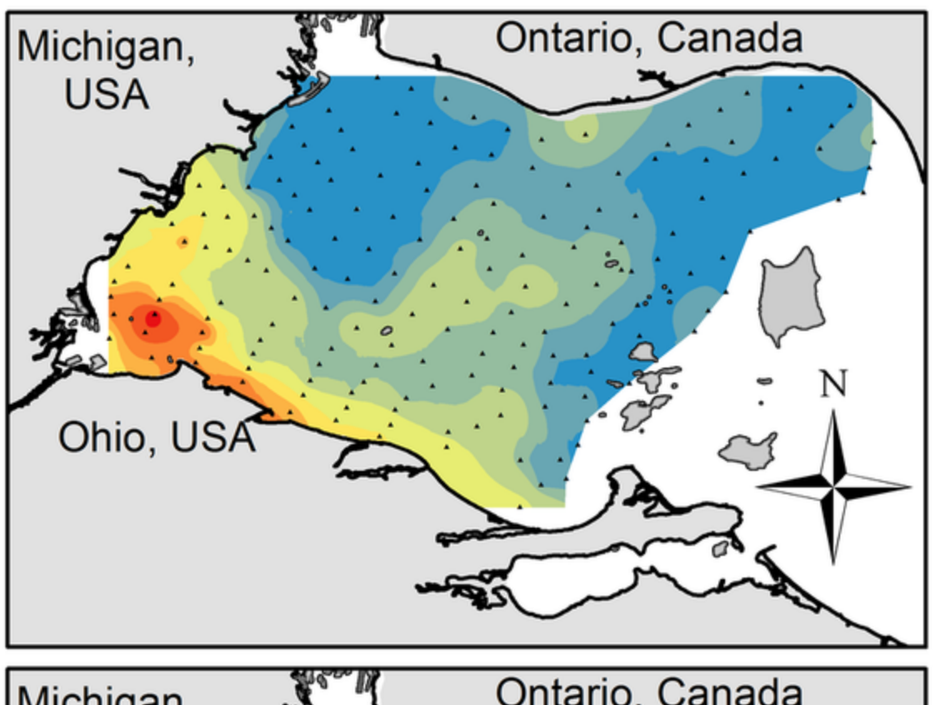
Michigan, USA
Ontario, Canada
Ohio, USA
N

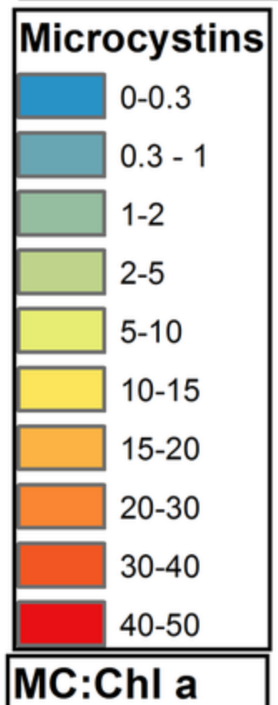
Microcystins
0-0.3
0.3 - 1
1-2
2-5
5-10
10-15
15-20
20-30
30-40
40-50

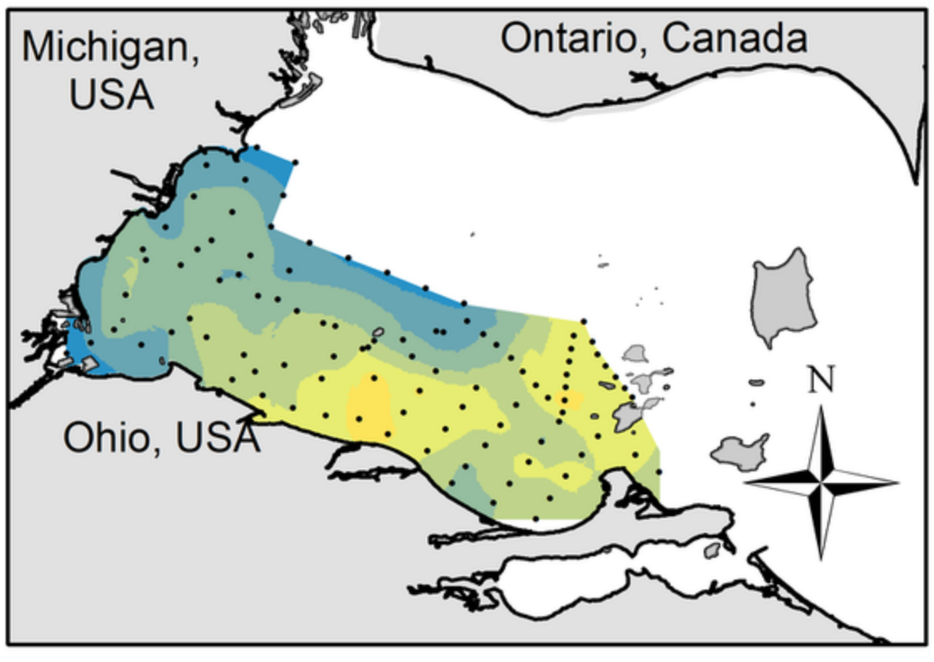
Michigan, USA
Ontario, Canada
Ohio, USA
N

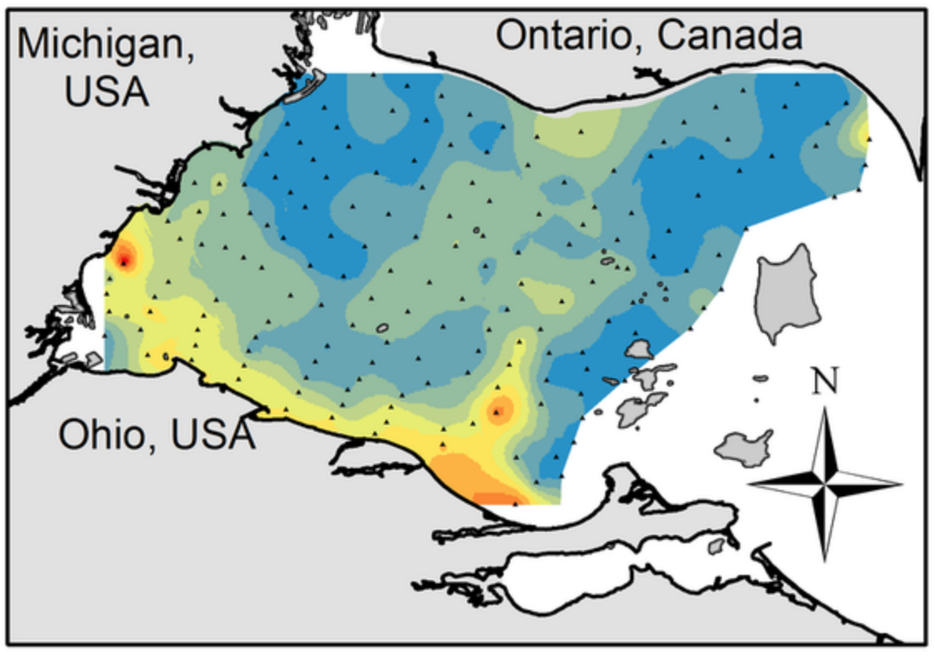
Michigan, USA
Ontario, Canada
Ohio, USA
N

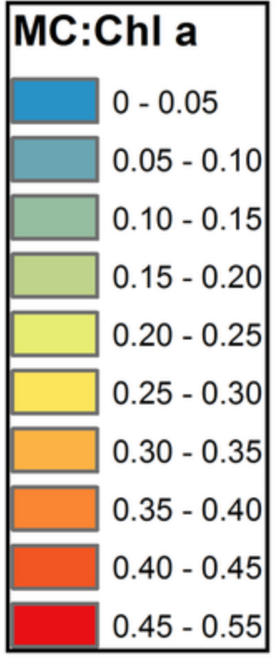
MC:Chl a
0 - 0.05
0.05 - 0.10
0.10 - 0.15
0.15 - 0.20
0.20 - 0.25
0.25 - 0.30
0.30 - 0.35
0.35 - 0.40
0.40 - 0.45
0.45 - 0.55

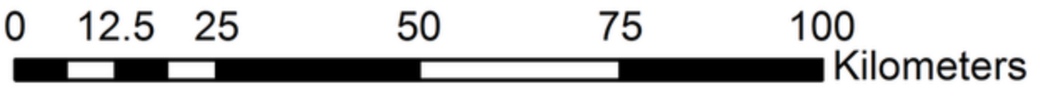
0
12.5
25
50
75
100
Kilometers

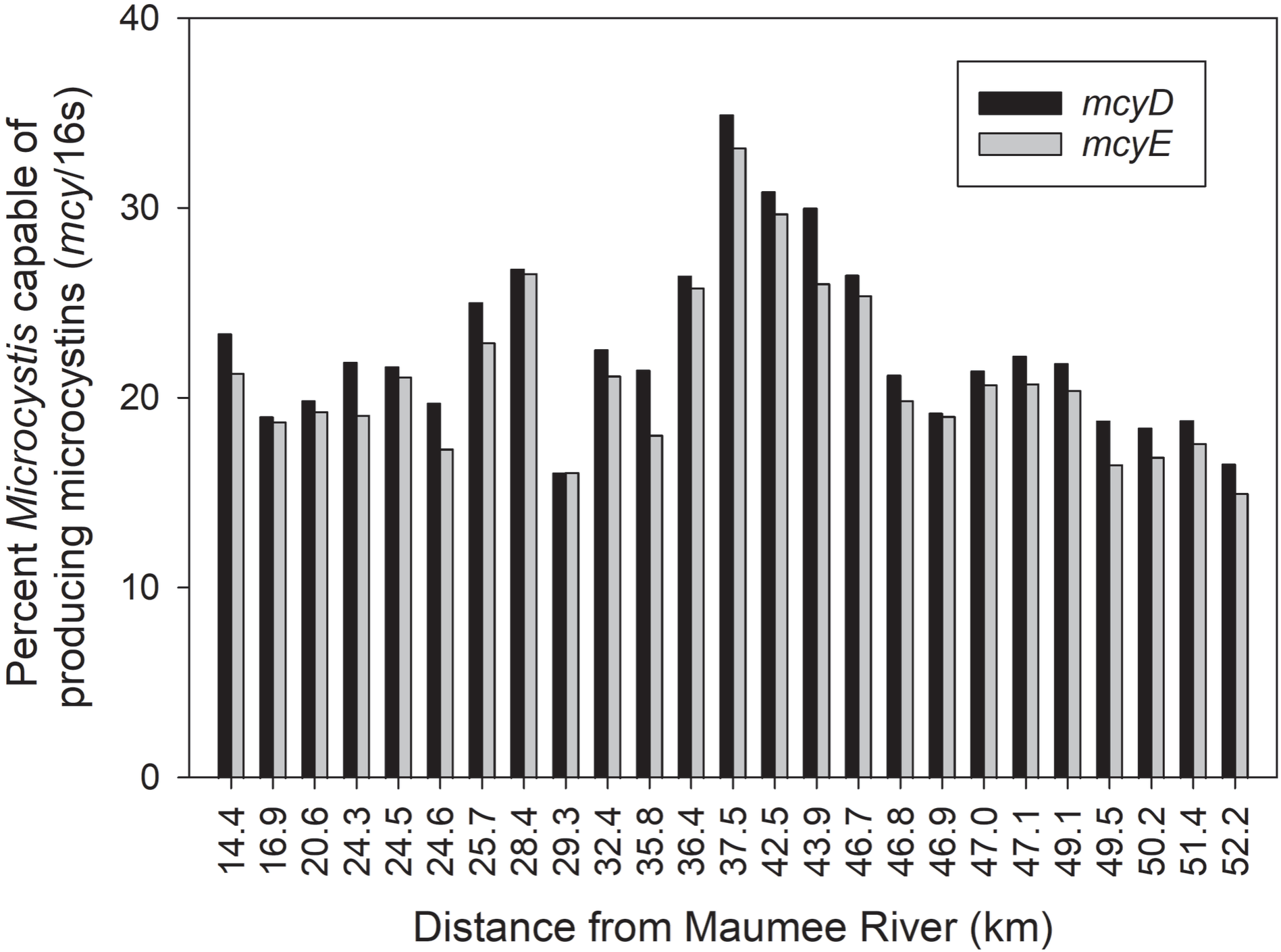
Percent Microcystis capable of producing microcystins (mcy/16s)
40
30
20
10
0
mcyD
mcyE
14.4
16.9
20.6
24.3
24.5
24.6
25.7
28.4
29.3
32.4
35.8
36.4
37.5
42.5
43.9
46.7
46.8
46.9
47.0
47.1
49.1
49.5
50.2
51.4
52.2
Distance from Maumee River (km)

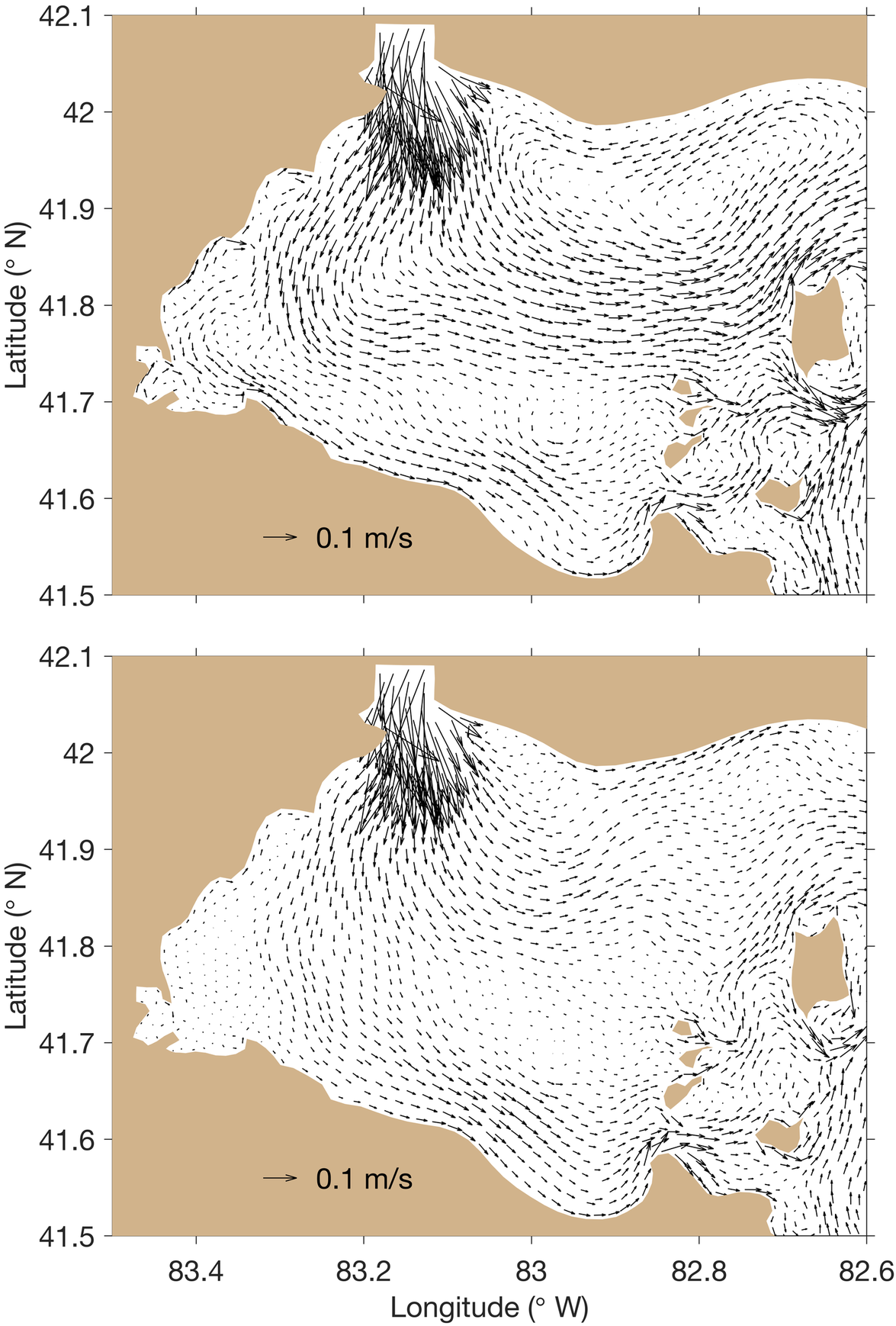
42.1
42
41.9
41.8
41.7
41.6
41.5
Latitude (° N)
0.1 m/s
42.1
42
41.9
41.8
41.7
41.6
41.5
Latitude (° N)
0.1 m/s
83.4
83.2
83
82.8
82.6
Longitude (° W)

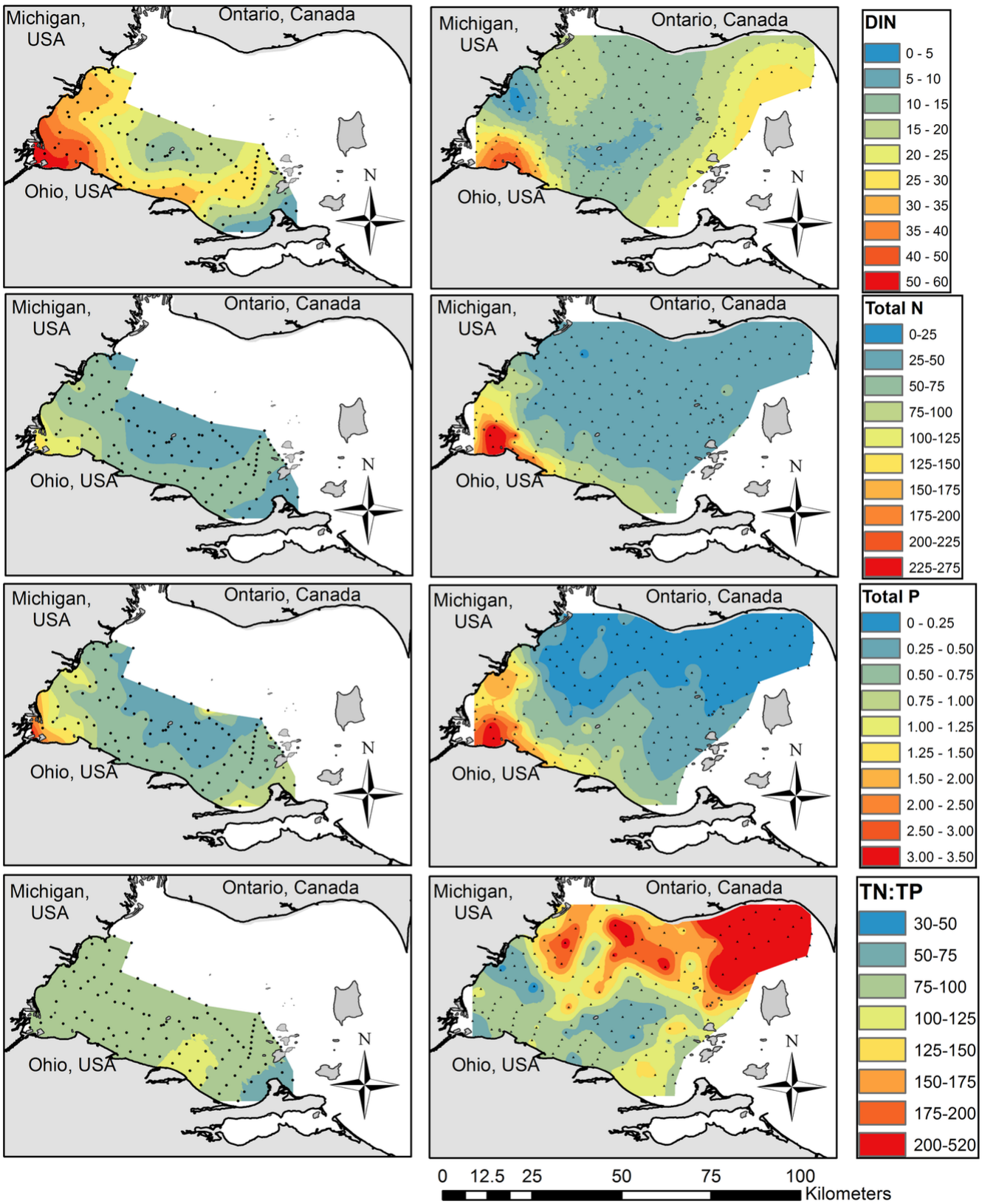
Michigan, USA
Ontario, Canada
Ohio, USA
N
DIN
0 - 5
5 - 10
10 - 15
15 - 20
20 - 25
25 - 30
30 - 35
35 - 40
40 - 50
50 - 60
Total N
0-25
25-50
50-75
75-100
100-125
125-150
150-175
175-200
200-225
225-275
Total P
0 - 0.25
0.25 - 0.50
0.50 - 0.75
0.75 - 1.00
1.00 - 1.25
1.25 - 1.50
1.50 - 2.00
2.00 - 2.50
2.50 - 3.00
3.00 - 3.50
TN:TP
30-50
50-75
75-100
100-125
125-150
150-175
175-200
200-520
0 12.5 25 50 75 100
Kilometers

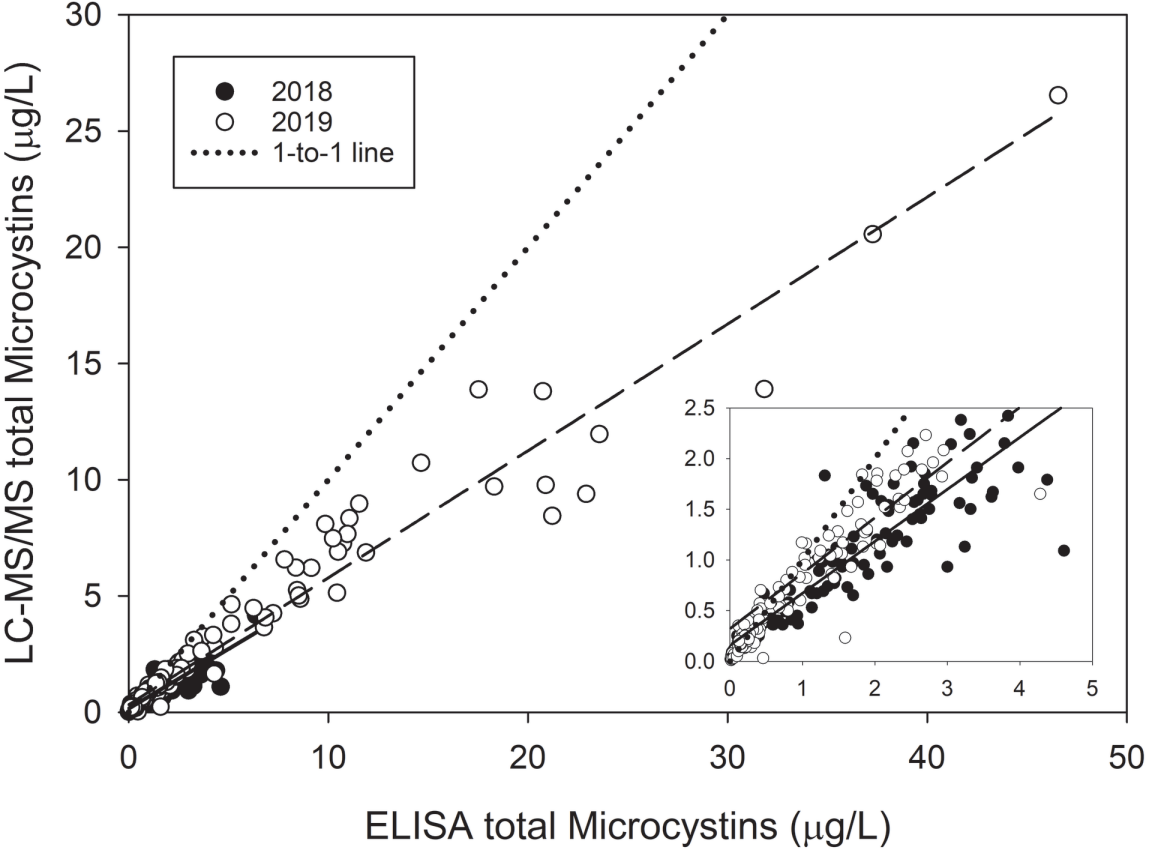
2018
2019
1-to-1 line
LC-MS/MS total Microcystins (μg/L)
ELISA total Microcystins (μg/L)
0
5
10
15
20
25
30
0
10
20
30
40
50
0.0
0.5
1.0
1.5
2.0
2.5
0
1
2
3
4
5

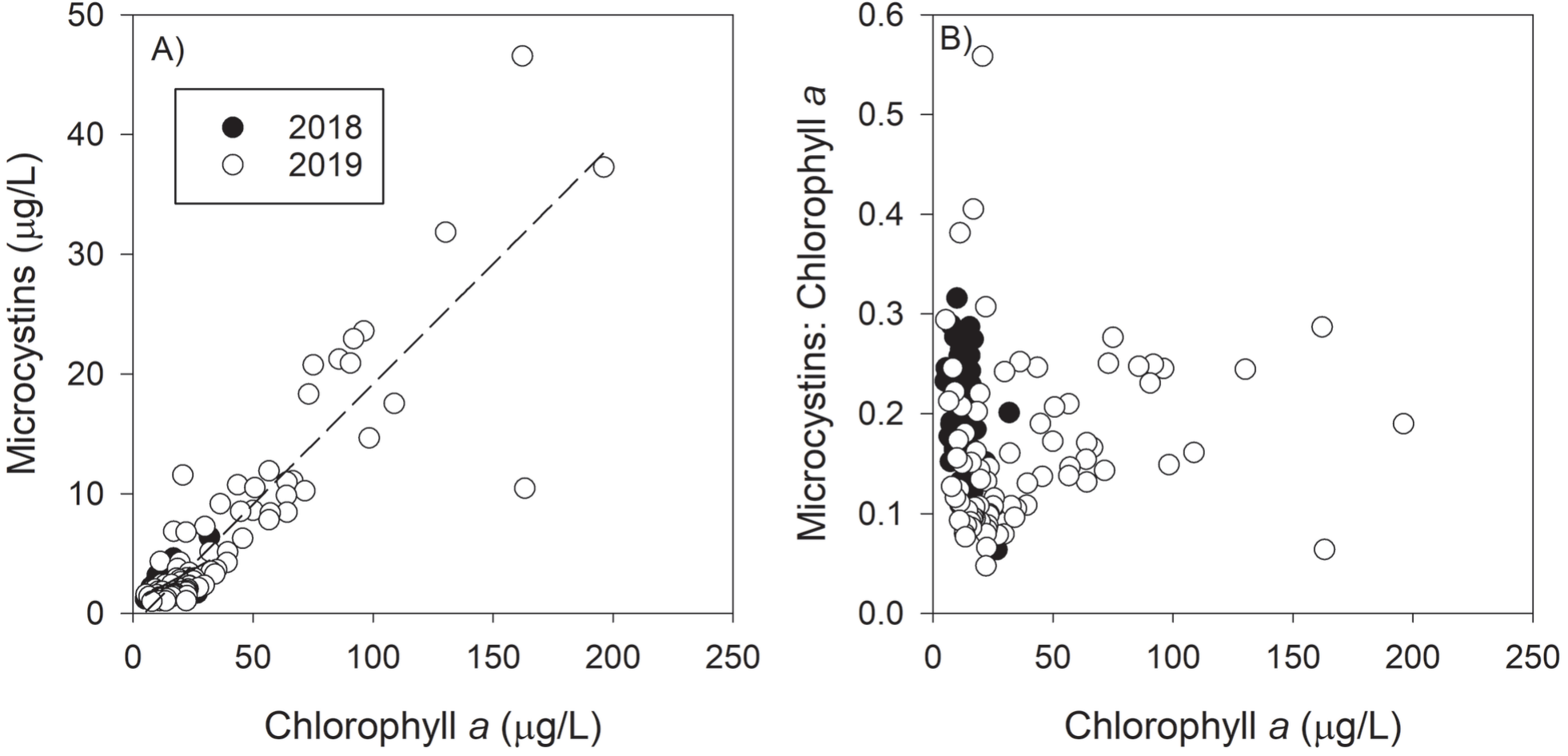
A)
2018
2019
Microcystins (µg/L)
Chlorophyll a (µg/L)
0
10
20
30
40
50
0
50
100
150
200
250
B)
Microcystins: Chlorophyll a
Chlorophyll a (µg/L)
0.0
0.1
0.2
0.3
0.4
0.5
0.6
0
50
100
150
200
250

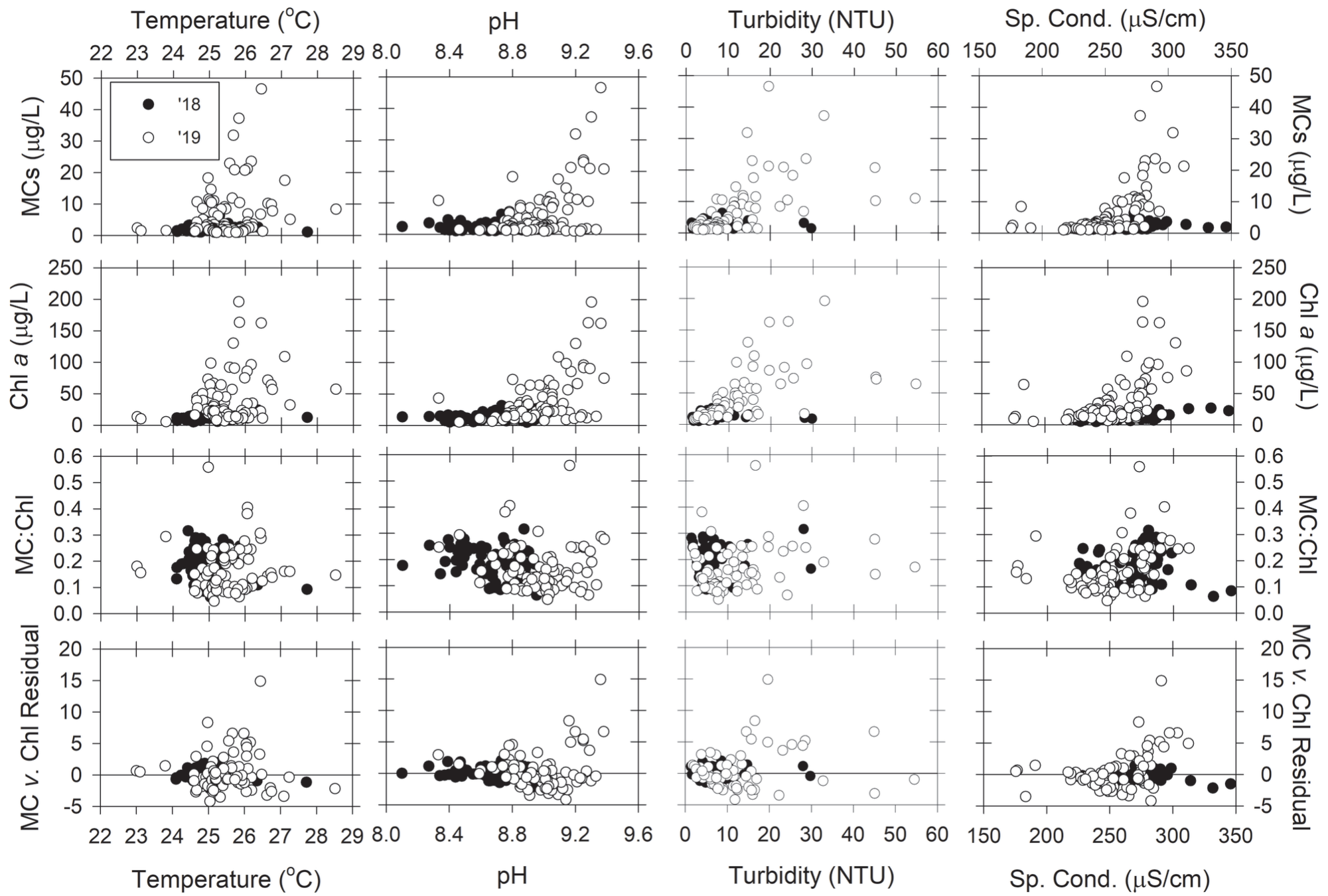
Temperature (°C)
pH
Turbidity (NTU)
Sp. Cond. (µS/cm)
'18
'19
MCs (µg/L)
Chl a (µg/L)
MC:Chl
MC v. Chl Residual

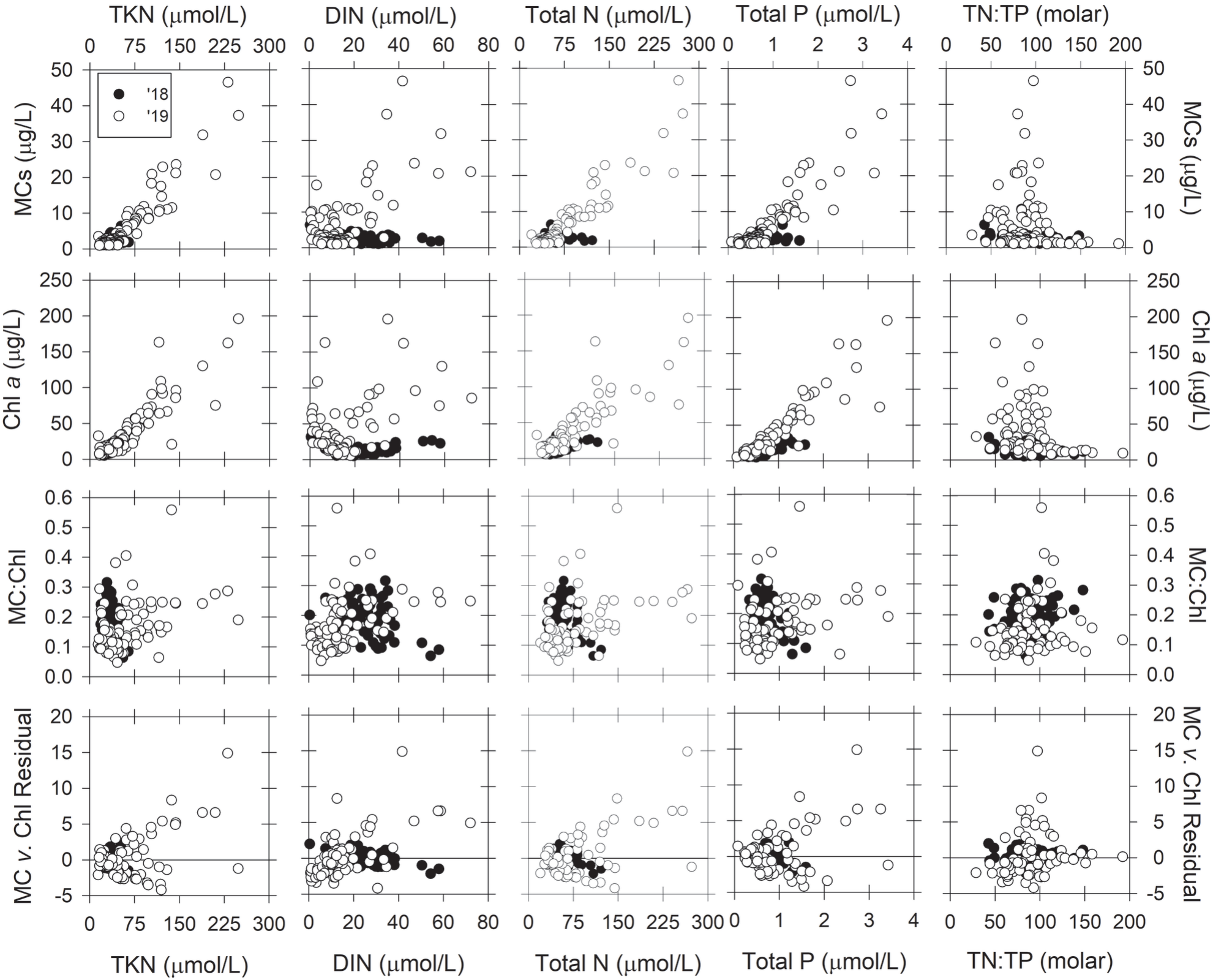
TKN (μmol/L)
DIN (μmol/L)
Total N (μmol/L)
Total P (μmol/L)
TN:TP (molar)
MCs (μg/L)
Chl a (μg/L)
MC:Chl
MC v. Chl Residual
'18
'19